submitted to *Geophys. J. Int.*

A model of elastic softening and second order phase transitions in anisotropic phases, with application to stishovite and post-stishovite

R. Myhill[1⋆]

[1]*School of Earth Sciences, University of Bristol. Wills Memorial Building, Queen's Road, Bristol BS8 1RJ*

SUMMARY

This paper introduces a comprehensive framework for modeling both instantaneous and time-dependent elastic softening in anisotropic materials. Like previous approaches, the framework employs Landau Theory, minimizing the Helmholtz energy by varying isochemical parameters ($\boldsymbol{q}$) that capture structural changes, atomic ordering, and/or electronic spin states. However, this model extends beyond earlier work by incorporating excess energy and anisotropic properties into an anisotropic solution model. This allows for fully self-consistent predictions of volume, unit cell parameters, the elastic tensor, and other thermodynamic properties as a function of pressure and temperature, while also accommodating large symmetry-breaking strains. The stishovite-to-post-stishovite transition is used as a case study to validate the formulation. It is demonstrated that, near this transition, both stishovite and post-stishovite exhibit auxetic behavior in several directions, with post-stishovite also displaying negative linear compressibility along the long axis of its unit cell.

Key words: Equations of state – Elasticity and anelasticity – Seismic anisotropy – Elastic softening

⋆ bob.myhill@bristol.ac.uk

1 INTRODUCTION

1.1 Isochemical variability in crystalline materials

The thermodynamic and elastic properties of crystalline phases are generally functions of the numbers of moles of independent chemical species $\boldsymbol{n}$ that comprise these phases. In many solutions, phases can be adequately modeled using only independent species that are compositionally independent of each other, such that there are the same number of independent chemical *components* $\boldsymbol{x}$ and independent chemical *species* $\boldsymbol{n}$. For example, $(Mg, Fe)_3Al_2Si_3O_{12}$ garnet (a two-component system, $n_x = 2$) can be reasonably modeled as a mixture of two species ($n_n = 2$): pyrope $[Mg]_3Al_2Si_3O_{12}$ and almandine $[Fe]_3Al_2Si_3O_{12}$. However, there are many pure phases and solid solutions whose properties can only be accurately modeled by explicitly considering one or more isochemical degrees of freedom $\boldsymbol{q}$. Three important types of isochemical degrees of freedom with examples involving a single degree of freedom are:

- Ordering: For example, Mg-Si exchange on two distinct octahedral sites in majorite (Heinemann et al., 1997):

$$q = (p_{\mathrm{Mg}^{\mathrm{M1}}} + p_{\mathrm{Si}^{\mathrm{M2}}}) - (p_{\mathrm{Si}^{\mathrm{M1}}} + p_{\mathrm{Mg}^{\mathrm{M2}}})$$

where, for example, $p_{\mathrm{Mg}^{\mathrm{M1}}}$ is the proportion of Mg on the M1 site.

- Electronic spin state: For example, variable proportions of high spin and low spin Fe^{2+} in ferropericlase (Wu et al., 2013) or troilite (Urakawa et al., 2004):

$$q = p_{\mathrm{Fe}^{\mathrm{M}}_{\mathrm{HS}}} - p_{\mathrm{Fe}^{\mathrm{M}}_{\mathrm{LS}}}$$

- Structural flexibility: For example, tilt angle Θ of tetrahedral SiO_4-units in quartz (Carpenter et al., 1998; Wells et al., 2002), or octahedral SiO_6-units in $CaCl_2$-structured post-stishovite (Zhang et al., 2023):

$$q = \Theta$$

While most materials exhibit monotonic changes in properties with changing pressure and temperature, materials with isochemical degrees of freedom $\boldsymbol{q}$ are often associated with anomalous thermodynamic and elastic properties.

1.2 Anomalous properties associated with isochemical variability

In one of the earliest observations of anomalous volumetric change, Le Chatelier (1890) noted that the unit cell volume of quartz increased rapidly with increasing temperature up to 570°C, and then actually decreased above 570°C. This peculiar behaviour is also accompanied by reduced elastic moduli (Car-

penter et al., 1998; Lakshtanov et al., 2007) and a peak in heat capacity (Grønvold & Stølen, 1992). The change in behaviour at 570°C is now known to mark a weakly first-order trigonal to hexagonal transition (e.g. Bachheimer & Dolino, 1975; Dolino, 1990; Antao, 2016). At low temperatures, the trigonal structure contains SiO_4 tetrahedra that are tilted relative to each other. As the structure is heated, the relative tilt angle decreases, and disappears at the transition. This change in tilt angle with temperature (and pressure) leads to the observed anomalies in physical properties in the trigonal phase. It turns out that the anomalous properties in the high-symmetry hexagonal phase are also related to tilting of SiO_4 tetrahedra, but in this case the anomalies are related to dynamic (thermally-driven) tilting, rather than static tilt in the trigonal phase (Welche et al., 1998; Wells et al., 2002).

Since the discovery of the anomalous properties of quartz, many other phases have been found to exhibit anomalous variations in heat capacities, thermal expansivities and elastic moduli (Helgeson, 1978; Thompson & Perkins, 1981; Wadhawan, 1982; Salje, 1985; Dove, 1997; Carpenter, 2006). These include some of the most abundant phases in the Earth: feldspar (Mookherjee et al., 2016; Lacivita et al., 2020), garnet (Heinemann et al., 1997), orthopyroxene (Jackson et al., 2004), amphibole (Cámara et al., 2003), cristobalite (Yeganeh-Haeri et al., 1992) stishovite (Kingma et al., 1995), ferropericlase (Wu et al., 2013) and $CaSiO_3$ perovskite (Stixrude et al., 2007). Many of the anomalies are associated with second order phase transitions. In all cases, the anomalous properties arise from the presence of one or more isochemical degrees of freedom in the crystalline structure.

1.3 Aim of this paper

The anomalous thermodynamic behaviour of materials has long been effectively described by models based on Landau Theory (e.g., Landau, 1935). These models, which rely on the concept of energy minimization by varying internal parameters $\boldsymbol{q}$, are successful due to their robust thermodynamic and group-theoretical foundation. However, despite their success, existing models of elastic behaviour have several limitations. Many sacrifice self-consistency in favour of simple expressions, or rely on simplifying assumptions, such as assuming small symmetry-breaking strains Tröster et al. (2002, 2014, 2017). Furthermore, most models are confined to either isobaric (Lüthi & Rehwald, 1981), or isothermal conditions (Carpenter et al., 2000; Tröster et al., 2014, 2017). High pressure, high temperature models are restricted to modelling only scalar properties (Angel et al., 2017).

The aim of the current paper is to develop a complete anisotropic theory that extends to high-pressure, high-temperature conditions and is not limited to small symmetry-breaking strains. Models based on this theory can take pressure, temperature and composition as input, and output any desired thermodynamic and elastic properties, such as the thermal expansivity or isentropic stiffness tensors.

The solution presented in this paper uses a new anisotropic solution equation of state (Myhill,

Table 1. Symbols used in this paper.

Symbol	Units	Description
$\mathcal{E}$, $\mathcal{F}$, $\mathcal{G}$, $\mathcal{H}$	J	Internal energy, Helmholtz energy, Gibbs energy, Enthalpy
$\boldsymbol{M}$, M_{ij}	m	The unit cell tensor scaled to the volume of the material
$\boldsymbol{F}$, F_{ij}	[unitless]	Deformation gradient tensor
$\boldsymbol{\sigma}$, σ_{ij}	Pa	Cauchy ("true") stress
$\boldsymbol{\varepsilon}$, ε_{ij}	[unitless]	Small strain tensor
$\hat{\boldsymbol{\varepsilon}}$, $\hat{\varepsilon}_{ij}$	[unitless]	Small strain tensor relative to the high-symmetry phase at fixed P and T
$\bar{\boldsymbol{\varepsilon}}$, $\bar{\varepsilon}_{ij}$	[unitless]	Non-hydrostatic isochoric small strain tensor
T	K	Temperature
S	J/K	Entropy
V	m^3	Volume
f	[unitless]	Logarithmic volume ($\ln(V/(1\ \mathrm{m}))$)
$\boldsymbol{n}$, n_i	mol	Molar amounts of compositional/structural endmembers
$\boldsymbol{p}$, p_i	[unitless]	Molar proportions of endmembers
$\boldsymbol{q}$, q_i	[unitless]	Isochemical degrees of freedom
$\boldsymbol{x}$, x_i	mol	Molar amounts of compositional/structural endmembers independent of relaxation vectors
$\boldsymbol{\mu}$	J/mol	Chemical potentials of endmembers
P	Pa	Pressure (-$\delta_{ij}\sigma_{ij}/3$)
$\boldsymbol{\pi}$, π_{ij}	Pa/K	Thermal stress tensor
$\mathbb{C}_{\mathrm{T}}$, $\mathbb{C}_{\mathrm{T}ijkl}$, $\mathbb{C}_{\mathrm{T}pq}$	Pa	Isothermal stiffness tensor (standard and Voigt form)
$\mathbb{C}_{\mathrm{S}}$, $\mathbb{C}_{\mathrm{S}ijkl}$, $\mathbb{C}_{\mathrm{S}pq}$	Pa	Isentropic stiffness tensor (standard and Voigt form)
$\boldsymbol{\alpha}$, α_{ij}; α_V	K^{-1}	Thermal expansivity tensor; Volumetric thermal expansivity
$C_{\boldsymbol{\sigma}}$, $C_{\boldsymbol{\varepsilon}}$, C_V, C_P	J/K	Isostress, isometric, hydrostatic-isochoric and isobaric heat capacities
β_{TR}, β_{SR}	Pa^{-1}	Isothermal and isentropic Reuss compressibilities
K_{TR}, K_{SR}	Pa	Isothermal and isentropic Reuss bulk moduli
$\boldsymbol{\gamma}$, γ_{ij}	[unitless]	Grüneisen tensor
Ψ, Ψ_{ijkl}	[unitless]	Anisotropic state tensor
$\boldsymbol{I}$, δ_{ij}		Identity matrix / Kronecker delta
$\ln_{\mathrm{M}}()$		Matrix logarithm function
$\exp_{\mathrm{M}}()$		Matrix exponential function

2024). Landau theory is incorporated into the solution model via non-ideal mixing between twin endmembers with the same bulk composition, thus mirroring order-disorder models that are used in many thermodynamic datasets (Holland & Powell, 2011; Stixrude & Lithgow-Bertelloni, 2024). Symbols used in this paper are provided in Table 1.

2 THEORETICAL MODEL DEVELOPMENT

2.1 Types of variables

Throughout this paper, the following terminology is applied to different types of variables:

- Natural variables: The independent variables or parameters that define a thermodynamic potential, such as the Gibbs energy $\mathcal{G}(\boldsymbol{\sigma}, T, \boldsymbol{x})$ (Nye et al., 1985; Holzapfel, 2000). Spontaneous processes within a system will tend to decrease the thermodynamic potential toward a minimum when the natural variables of that potential are held constant.
- Internal variables: Variables that describe the internal state of the system but are not necessarily controlled or directly manipulated from outside the system. Variation of these variables allows the thermodynamic potential to approach a minimum. In this paper, internal variables are indicated by the symbol $\boldsymbol{q}$.
- Conjugate variables: The derivatives of the thermodynamic potentials with respect to their natural variables. These are related to properties of the system. For example, Cauchy stress is related to the first derivative of the Helmholtz energy with respect to strain:

$$\left(\frac{\partial \mathcal{F}}{\partial \varepsilon_{ij}}\right)_{T,\boldsymbol{x}} = V\sigma_{ij} \tag{1}$$

$$d\varepsilon_{ij} = \frac{1}{2}(dF_{ik}F_{jk}^{-1} + dF_{jk}F_{ik}^{-1}) \tag{2}$$

2.2 Landau Theory

In the 1930s, Landau wrote a series of papers that explained the origin of anomalous peaks in heat capacity and other phenomena involving continuous transitions (Landau, 1935, 1937a,b). See English translations in (Landau, 2008; Ter Haar, 2013). Landau (1935) theorised that such peaks were a natural consequence of minimizing energy by varying an internal variable q. To demonstrate his theory, he constructed a thermodynamic potential Φ as a polynomial relative to a reference state:

$$\Phi = \Phi_0 + aq + bq^2 + cq^3 + \dots \tag{3}$$

where Φ_0, a, b, c, ... are all potentially functions of the natural variables of Φ. Landau implicitly used the Gibbs energy ($\mathcal{G}(P, T, \boldsymbol{x})$; e.g. Landau, 1935) and Helmholtz energy ($\mathcal{F}(V, T, \boldsymbol{x})$; e.g. Landau & Ginzburg, 1950) as convenient thermodynamic potentials for different problems.

Landau later showed that symmetry-breaking transitions could be modeled using an energy expansions that were symmetric about $q = 0$, with Φ_0 representing the energy of the high-symmetry phase (Landau, 1937a):

$$\Phi = \Phi_0 + bq^2 + dq^4 + \dots \tag{4}$$

If $\partial^2\Phi/\partial q\partial q > 0$ at $q = 0$, then the high-symmetry state is more stable than states where the symmetry is slightly broken. The high-symmetry state may then represent the globally stable state. Conversely, if $\partial^2\Phi/\partial q\partial q < 0$, then the high-symmetry state is less stable than the low symmetry form, and two local minima in the energy will appear at positive and negative q, corresponding to twin structures. If a change in conditions causes $q = 0$ to lose or gain its status as the global minimum, a symmetry-breaking transition takes place.

Landau (1937a) motivated his use of a single internal variable q to describe symmetry breaking as follows. Let the probability density function of different atoms as a function of spatial position be equal to $\boldsymbol{\rho} = \boldsymbol{\rho}(x, y, z)$. Furthermore, let the difference between the equilibrium and high-symmetry structures be equal to $\delta\boldsymbol{\rho}$. The perturbation $\delta\boldsymbol{\rho}$ can be split into a number of normalised irreducible functions (i.e., a basis set of functions) $\boldsymbol{I}_i$ that satisfy the symmetry of the parent group - subgroup transition (Stokes & Hatch, 1988; Powell, 2010):

$$\delta\boldsymbol{\rho}(x, y, z) = \sum_i c_i \boldsymbol{I}_i(x, y, z) \tag{5}$$

The excess energy Φ_{xs} can given as a function of $\delta\boldsymbol{\rho}$ or, equivalently, by the values of c_i:

$$\Phi_{\text{xs}} = \Phi_{\text{xs}}(\boldsymbol{c}) \tag{6}$$

The vector of internal variables $\boldsymbol{c}$ potentially has a large number of components. To simplify the system, we assume that all the accessible values of $\boldsymbol{c}$ at any given state lie along some line in $\boldsymbol{c}$-space, and that the distance along this line from the origin can be parameterised by a single variable q. It is then possible to write both Φ and $\boldsymbol{c}$ as a function of this parameter:

$$\Phi = \Phi_0 + \Phi_{\text{xs}}(q),\ \boldsymbol{c} = \boldsymbol{c}(q) \tag{7}$$

The excess energy Φ_{xs} can then be expanded in powers of q, as in Equation 4. In Landau (1937a), $q^2 = \sum c_i^2$, but such a restrictive choice is not required.

2.3 Coupled models of elastic strain around phase transitions

The models considered by Landau focused on the evolution of systems as a function of temperature. Subsequent models, informed by work on piezoelectrics and ferroelectrics such as Rochelle Salt (Mueller, 1940; Ginzburg, 1945; Devonshire, 1949), started to consider both systems with more than one natural variable, and also systems where conjugate variables were constrained, rather than the natural variables. The resulting "Landau-Ginzburg-Devonshire Theory" (Levanyuk & Sannikov, 1969, 1970, 1971) has been applied to studies of elastic effects during second-order transitions since the 1970s (Dvořák, 1971; Höchli, 1972; Lüthi & Rehwald, 1981; Kityk et al., 2000). Under unstressed

conditions ($\boldsymbol{\sigma} = \mathbf{0}$), and with one internal variable (q) the Helmholtz energy in the small strain approximation can be written as a set of simultaneous equations:

$$\mathcal{F}(T, \hat{\boldsymbol{\varepsilon}}, q) = \mathcal{F}_0(T) + V\left(bq^2 + dq^4 + fq^6 \ldots + \sum_{ij,m,n} \lambda_{i,m,n}\hat{\varepsilon}_i^m q^n + \frac{1}{2}\sum_{i,k} \mathbb{C}^0_{ik}\hat{\varepsilon}_i\hat{\varepsilon}_k\right) \tag{8}$$

$$\frac{\partial \mathcal{F}}{\partial \hat{\varepsilon}_{ij}} = 0_{ij}\,(= V\sigma_{ij}) \tag{9}$$

where b, d, f, $\lambda_{i,m,n}$, $\mathbb{C}^0_{ik}$, ... are all potentially functions of temperature, $\hat{\boldsymbol{\varepsilon}}$ is strain relative to the high-symmetry form, and "strain-order coupling" coefficients $\lambda_{i,m,n}$ are only non-zero when allowed by the symmetry of the system (Carpenter & Salje, 1998). In this expression, T and $\hat{\boldsymbol{\varepsilon}}$ are natural variables of the system. By substituting Equations 9 back into Equation 8, a classic Landau-type expression is recovered:

$$\mathcal{F}(T, q) = \mathcal{F}_0(T) + V\left(b'q^2 + d'q^4 + f'q^6 + \ldots\right) \tag{10}$$

where the modified coefficients b', d' and f' are functions of b, d, f, $\lambda_{i,m,n}$ and $\mathbb{C}^0_{ik}$.

Attempts have been made to apply this theory to phase transitions at high pressure. Some studies (Liakos & Saunders, 1982; Carpenter et al., 2000; Buchen, 2021; Zhang et al., 2021a), use Equations 8 and 9 essentially unaltered, except that the Helmholtz energies are re-labelled as Gibbs energies, and $\mathcal{F}_0$ (now $\mathcal{G}_0$) becomes a function of pressure rather than temperature. The derivative of the energy with respect to strain (Equation 9) is set to zero. This method is successful at reproducing observed changes in elastic tensor, but the formulation is thermodynamically inconsistent and produces conflicting estimates of physical properties such as the volume (see Supplementary Information). To achieve thermodynamic consistency in the small strain limit, Tröster et al. (2014, 2017) introduced an additional $\sigma_{ij}\varepsilon_{ij}$ term to Equation 8, and set $\partial\mathcal{F}/\partial\hat{\boldsymbol{\varepsilon}} = V\boldsymbol{\sigma}$. The use of this formulation still requires self-consistent expressions for the Helmholtz energy, cell tensor $\boldsymbol{M}$ and isothermal stiffness tensor $\mathbb{C}_T$ of the high-symmetry phase as a function of pressure and, ideally, temperature, which is prohibitively complex using classic expansions in finite strain (Tröster et al., 2017).

2.4 A general equation of state for anisotropic phases under near-hydrostatic conditions

In a companion paper (Myhill, 2024), I proposed a self-consistent anisotropic equation of state for solid solutions that provided expressions for the Helmholtz energy, cell tensor $\boldsymbol{M}$ and isothermal stiffness tensor $\mathbb{C}_T$ as a function of volume V, temperature T, endmember proportions $\boldsymbol{n}$ and small

isochoric strain $\bar{\boldsymbol{\varepsilon}}$:

$$\mathcal{F}(V,T,\boldsymbol{n},\bar{\boldsymbol{\varepsilon}}) = \mathcal{F}_{\text{hyd}}(V,T,\boldsymbol{n}) + \mathcal{F}_{\text{el}}(V,T,\boldsymbol{n},\bar{\boldsymbol{\varepsilon}}) \tag{11}$$

$$M_{ij}(V,T,\boldsymbol{n},\bar{\boldsymbol{\varepsilon}}) = (\delta_{ik} + \bar{\varepsilon}_{ik})F_{kl}(V,T,\boldsymbol{n})M_{0lj}(\boldsymbol{n}) \tag{12}$$

$$\mathcal{F}_{\text{el}}(V,T,\boldsymbol{n},\bar{\boldsymbol{\varepsilon}}) = \frac{1}{2}V\sum_{i,j}\bar{\varepsilon}_i\mathbb{C}_{\text{T,hyd}ij}(V,T,\boldsymbol{n})\bar{\varepsilon}_j \tag{13}$$

The hydrostatic part of the Helmholtz energy $\mathcal{F}_{\text{hyd}}(V,T,\boldsymbol{n})$ can be calculated from any scalar equation of state. If pressure is a more convenient independent variable than volume, the Helmholtz energy can be calculated from an equation of state formulated as $\mathcal{G}_{\text{hyd}}(P,T,\boldsymbol{n})$:

$$\mathcal{F}_{\text{hyd}} = \mathcal{G}_{\text{hyd}}(P,T,\boldsymbol{n}) - P\,V(P,T,\boldsymbol{n}) \tag{14}$$

$$V = \frac{\partial\mathcal{G}_{\text{hyd}}(P,T,\boldsymbol{n})}{\partial P} \tag{15}$$

Self consistency of the anisotropic and scalar properties of the equation of state in orthotropic materials is guaranteed by use of a fourth order tensor Ψ, related to the deformation gradient tensor and compliance tensor:

$$F_{ij}(V,T,\boldsymbol{n}) = (\exp_{\text{M}}\Psi(V,T,\boldsymbol{n})\boldsymbol{I})_{ij} \tag{16}$$

$$\left(\frac{S_{\text{T}ijkl}}{\beta_{\text{RT}}}\right)_{\boldsymbol{n}} = \left(\frac{\partial\psi_{ijkl}}{\partial\ln V}\right)_{T,\boldsymbol{n}} \tag{17}$$

This equation of state can be used to provide all of the properties required for the reference properties of the high-symmetry phase in the formulation of Tröster et al. (2014, 2017) (Section 2.3). However, we can do better than this, by also using the equation of state to resolve the small strain limitation of the Tröster et al. (2014, 2017) theory. To do this, we use linear transformation to decompose the endmember proportions $\boldsymbol{n}$ into natural variables $\boldsymbol{x}$ and internal variables $\boldsymbol{q}$ (Myhill & Connolly, 2021):

$$dn_i = A_{ij}dq_j + B_{ik}dx_k \tag{18}$$

where $\boldsymbol{A}$ and $\boldsymbol{B}$ are constant transformation matrices. As the Myhill (2024) formalism already provides expressions for the unit cell tensor $\boldsymbol{M}$ and elastic tensor $\mathbb{C}_{\text{T}}$ in terms of V, T and $\boldsymbol{n}$ (Equations 12, 17), it is unnecessary to constrain or solve a system of equations for the symmetry-breaking strain $\hat{\boldsymbol{\varepsilon}}$ (Equation 9). The Landau expansion coefficients (Figure 10) do not need to be functions of any "strain-order coupling" coefficients, or of the reference stiffness tensor.

We shall use the Myhill (2024) equation of state to investigate the stishovite to post-stishovite transition in Section 4. However, first, we must quantify the effect of dynamic changes in $\boldsymbol{q}$ on second derivatives of the thermodynamic potential such as the elastic compliance tensor.

3 THE EFFECT OF MATERIAL PROPERTIES

3.1 Relationships between state, material properties and thermodynamic potentials

The beauty of thermodynamics is that observable properties of materials arise from the partial derivatives of thermodynamic potentials with respect to their natural variables. Taking the Helmholtz energy ($\mathcal{F} = \mathcal{F}(\boldsymbol{M}, T, \boldsymbol{n})$) as an example, first derivatives with respect to the natural variables define the Cauchy stress $\boldsymbol{\sigma}$, entropy S and chemical potentials μ_i:

$$d\mathcal{F} = \frac{\partial \mathcal{F}}{\partial \varepsilon_{ij}} d\varepsilon_{ij} + \frac{\partial \mathcal{F}}{\partial T} dT + \frac{\partial \mathcal{F}}{\partial n_i} dn_i \tag{19}$$

$$= V\sigma_{ij} d\varepsilon_{ij} - SdT + \mu_i dn_i \tag{20}$$

$$d\varepsilon_{ij} = \frac{1}{2}(dM_{ik} M^{-1}_{jk} + dM_{jk} M^{-1}_{ik}) \tag{21}$$

where $\boldsymbol{\varepsilon}$ is the small strain tensor. The work term can be further split into volumetric and rotation-free, isochoric strain $\bar{\boldsymbol{\varepsilon}}$ (Holzapfel, 2000):

$$d\mathcal{F} = -PdV + V\tau_{ij} d\bar{\varepsilon}_{ij} - SdT + \mu_i dn_i \tag{22}$$

The second derivatives of the Helmholtz energy with respect to strain and temperature at fixed bulk composition $\boldsymbol{x}$ yield the isothermal stiffness tensor ($\mathbb{C}_\mathrm{T}$), the thermal stress tensor ($\boldsymbol{\pi}$, that describes how internal stress changes with temperature if deformation is not allowed to occur) and the isometric heat ($C_{\boldsymbol{\varepsilon}}$):

$$\left(\frac{\partial^2 \mathcal{F}}{\partial \varepsilon_{ij} \partial \varepsilon_{kl}}\right)_{\boldsymbol{x}, T, \varepsilon_{mn \neq ij,kl}} = V\mathbb{C}_{\mathrm{T}ijkl} \tag{23}$$

$$\left(\frac{\partial^2 \mathcal{F}}{\partial \varepsilon_{ij} \partial T}\right)_{\boldsymbol{x}, \varepsilon_{kl \neq ij}} = V\pi_{ij} \tag{24}$$

$$\left(\frac{\partial^2 \mathcal{F}}{\partial T \partial T}\right)_{\boldsymbol{x}, \boldsymbol{\varepsilon}} = -\frac{C_{\boldsymbol{\varepsilon}}}{T} \tag{25}$$

Note that in these expressions we have not specified whether the internal variables $\boldsymbol{q}$ are fixed or allowed to vary. This will be the subject of the next section. Other thermodynamic properties may be determined through appropriate algebraic manipulation (Davies, 1974; Nye et al., 1985; Holzapfel,

2000):

$$\mathbb{C}_{\mathrm{S}} = \mathbb{C}_{\mathrm{T}} + \frac{VT}{C_{\boldsymbol{\varepsilon}}}\boldsymbol{\pi}\boldsymbol{\pi} \tag{26}$$

$$\mathbb{S}_{\mathrm{T}} = (\mathbb{C}_{\mathrm{T}})^{-1}; \quad \mathbb{S}_{\mathrm{S}} = (\mathbb{C}_{\mathrm{S}})^{-1} \tag{27}$$

$$\beta_{\mathrm{TR}} = \boldsymbol{I}\mathbb{S}_{\mathrm{T}}\boldsymbol{I}; \quad \beta_{\mathrm{SR}} = \boldsymbol{I}\mathbb{S}_{\mathrm{S}}\boldsymbol{I} \tag{28}$$

$$\boldsymbol{\alpha} = -\mathbb{S}_{\mathrm{T}}\boldsymbol{\pi}; \quad \alpha_V = \mathrm{Tr}(\boldsymbol{\alpha}) \tag{29}$$

$$C_{\boldsymbol{\sigma}} = C_{\boldsymbol{\varepsilon}} + VT\boldsymbol{\alpha}\mathbb{C}_{\mathrm{T}}\boldsymbol{\alpha} = C_{\boldsymbol{\varepsilon}} - VT\boldsymbol{\alpha}\boldsymbol{\pi} \tag{30}$$

$$\boldsymbol{\gamma} = \mathbb{C}_{\mathrm{S}}\boldsymbol{\alpha}\frac{V}{C_{\boldsymbol{\sigma}}} \tag{31}$$

Under hydrostatic conditions, the following scalar properties can be defined using the properties defined above:

$$C_P = C_{\boldsymbol{\sigma}} = \frac{VT\alpha_V^2}{(\beta_{\mathrm{TR}} - \beta_{\mathrm{SR}})} \tag{32}$$

$$C_V = C_P\frac{\beta_{\mathrm{SR}}}{\beta_{\mathrm{TR}}} \tag{33}$$

$$\gamma = \frac{\alpha_V V}{\beta_{\mathrm{SR}} C_P} \tag{34}$$

See Appendix A for derivations of Equations 26, 29 and 30.

3.2 The concept of relaxation

As the state of a system changes, a change in the internal variables $\boldsymbol{q}$ might be able to reduce the appropriate potential (or, in other words, increase the entropy of the universe). Some changes, such as tilting of structural units or changes in electronic spin state are extremely rapid with respect to the rate of changes in stress and temperature (Slonczewski & Thomas, 1970; Kimizuka et al., 2003; Zhang et al., 2018). In contrast, order-disorder processes are often sluggish because the activation energy required for the migration of chemical species is larger than the average thermal energy of these species (Seifert & Virgo, 1975; Ganguly, 1982; Redfern, 1998; Redfern et al., 1999; Redfern, 2000). If $\boldsymbol{q}$ are not allowed to change during changes in state, then we can define the "unrelaxed" properties of the system:

$$\left(\frac{\partial^2\mathcal{F}}{\partial\varepsilon_{ij}\partial\varepsilon_{kl}}\right)_{\boldsymbol{q},\boldsymbol{x},T,\varepsilon_{mn\neq ij,kl}} = V\mathbb{C}_{\mathrm{T}ijkl}^{\text{unrelaxed}} \tag{35}$$

$$\left(\frac{\partial^2\mathcal{F}}{\partial\varepsilon_{ij}\partial T}\right)_{\boldsymbol{q},\boldsymbol{x},\varepsilon_{kl\neq ij}} = V\pi_{ij}^{\text{unrelaxed}} \tag{36}$$

$$\left(\frac{\partial^2\mathcal{F}}{\partial T\partial T}\right)_{\boldsymbol{q},\boldsymbol{x},\boldsymbol{\varepsilon}} = -\frac{1}{T}C_{\boldsymbol{\varepsilon}}^{\text{unrelaxed}} \tag{37}$$

Table 2. Variable sets used in this paper. For the meaning of each variable, see Table 1.

Set	Identifier	Independent variables	Section of first appearance
Anisotropic EoS	$\ldots'$	$V, T, \boldsymbol{n}, \bar{\varepsilon}$	2.4
Gibbs energy (hydrostatic)	$\ldots^{\mathcal{G}}$	$P, T, \boldsymbol{n}$	2.4
Helmholtz ("unrelaxed")	$\ldots$	$\boldsymbol{M}, T, \boldsymbol{n}$	3.1
Helmholtz ("relaxed")	$\ldots^*$	$\boldsymbol{M}, T, \boldsymbol{x}$	3.3.1
Internal energy	$\ldots^{\mathcal{E}}$	$\boldsymbol{M}, S, \boldsymbol{n}$	3.4

If $\boldsymbol{q}$ responds rapidly to minimise energy compared with the timescales over which the natural variables change, then a set of modified second derivatives can be defined, and these are referred to as "relaxed" properties (Section 3.3). Between these two endmember cases, there is an intermediate situation where changes in $\boldsymbol{q}$ take place on similar timescales to changes in state, in which case the material can be described as partially relaxed (Section 3.4).

In this paper, different thermodynamic potentials and sets of variables are needed to solve various relaxation problems. For instance, the anisotropic equation of state described in Section 2.4 has V, T, $\boldsymbol{n}$, and $\bar{\varepsilon}$ as its natural variables. However, relaxed properties are more conveniently expressed as partial derivatives with respect to the variables $\boldsymbol{M}$, T and $\boldsymbol{n}$. Seismic properties, on the other hand, are determined under conditions of constant entropy S, rather than constant temperature T. In thermodynamic calculations, it is important to know which parameters are varied and which are held constant when performing partial differentiation. Instead of repeatedly using subscripts to indicate what is held constant (e.g., $()_T$), in the following sections, superscripts will be used to denote variables from different sets. These variable sets are summarised in Table 2.

3.3 The properties of a rapidly relaxed elastic material

3.3.1 Variational calculus

In the endmember scenario that one or more isochemical order parameters $\boldsymbol{q}$ change instantaneously to minimise $\mathcal{F}$ under small changes in strain and temperature, variational calculus can be used to calculate relaxed properties. Relaxed values of $\boldsymbol{q}$ (denoted $\boldsymbol{q}^*$) are therefore a function of the other variables of the system:

$$\boldsymbol{q}^* = \boldsymbol{q}^*(\boldsymbol{M}, T, \boldsymbol{x}) \tag{38}$$

For small, rotation-free perturbations about a hydrostatic state $\boldsymbol{M}_0$ (such that $\boldsymbol{M} = (\boldsymbol{I} + \boldsymbol{\varepsilon})\boldsymbol{M}_0$), we can consider the small strain tensor only

$$\boldsymbol{q}^* = \boldsymbol{q}^*(\boldsymbol{\varepsilon}, T, \boldsymbol{x}) \tag{39}$$

Collecting small strain and temperature together as $\boldsymbol{z} = \{\boldsymbol{\varepsilon}, T\}$, the change in $\boldsymbol{q}^*$ with change in $\boldsymbol{z}$ at fixed $\boldsymbol{x}$ can be determined using the following expression (Appendix B):

$$\frac{\partial q_k^*}{\partial z_j} = -R_{kl}\frac{\partial^2 \mathcal{F}}{\partial q_l \partial z_j} \tag{40}$$

where $\boldsymbol{R}$ is the left inverse matrix of $\partial^2\mathcal{F}/\partial q_l \partial q_m$:

$$\delta_{km} = R_{kl}\frac{\partial^2 \mathcal{F}}{\partial q_l \partial q_m} \tag{41}$$

The relationship between the relaxed and unrelaxed second derivatives of the Helmholtz energy with respect to state is then given by the following expressions:

$$\frac{\partial^2 \mathcal{F}^*}{\partial z_i \partial z_j} = \frac{\partial^2 \mathcal{F}}{\partial z_i \partial z_j} + \frac{\partial^2 \mathcal{F}}{\partial z_i \partial q_k}\frac{\partial q_k^*}{\partial z_j} \tag{42}$$

$$\left[\begin{array}{c|c} V\mathbb{C}_{\mathrm{T}}^* & V\boldsymbol{\pi}^* \\ \hline V\boldsymbol{\pi}^{*\mathrm{T}} & -C_{\boldsymbol{\varepsilon}}^*/T \end{array}\right]_{ij} = \left[\begin{array}{c|c} V\mathbb{C}_{\mathrm{T}} & V\boldsymbol{\pi} \\ \hline V\boldsymbol{\pi}^{\mathrm{T}} & -C_{\boldsymbol{\varepsilon}}/T \end{array}\right]_{ij} + \frac{\partial^2 \mathcal{F}}{\partial z_i \partial q_k}\frac{\partial q_k^*}{\partial z_j} \tag{43}$$

The values of $\boldsymbol{q}^*$ are state properties; they have unique values as a function of $\boldsymbol{M}$, T, $\boldsymbol{x}$ and do not depend on the path taken to achieve that state. Therefore, the properties calculated in Equation 43, which correspond to relaxed properties at fixed strain and temperature, can be used in combination with the equations in Section 3.1 to determine other relaxed properties at fixed entropy or stress. For example, the equation for the relaxed isentropic stiffness tensor can be written:

$$\mathbb{C}_{\mathrm{S}}^* = \mathbb{C}_{\mathrm{T}}^* + \frac{VT}{C_{\boldsymbol{\varepsilon}}^*}\boldsymbol{\pi}^*\boldsymbol{\pi}^* \tag{44}$$

which is directly analogous to the unrelaxed expression (Equation 26).

3.3.2 Change of variables

Equations 40, 41 and 43 require the derivatives of $\mathcal{F}$ with respect to $\boldsymbol{\varepsilon}$, T and $\boldsymbol{q}$, but the equation of state from Myhill (2024) is expressed as $\mathcal{F}(V', T', \boldsymbol{n}', \bar{\boldsymbol{\varepsilon}}')$ (Section 2.4, Table 2). The required derivatives can be calculated by a change of variables (Appendix C):

$$\frac{\partial^2 \mathcal{F}}{\partial q_i \partial q_j} = A_{ui}\left(H_{uv}^{\mathcal{F}} + V\frac{\partial \varepsilon_{mn}}{\partial n_u'}\mathbb{C}_{\mathrm{T}mnpq}\frac{\partial \varepsilon_{pq}}{\partial n_v'}\right)A_{vj} \tag{45}$$

$$\frac{\partial^2 \mathcal{F}}{\partial q_i \partial T} = A_{ui}\left(-\frac{\partial S}{\partial n_u'} + V\frac{\partial \varepsilon_{mn}}{\partial n_u'}\mathbb{C}_{\mathrm{T}mnpq}\left(\frac{\alpha_{pq}}{\alpha_V} - \frac{\beta_{\mathrm{T}pq}}{\beta_{\mathrm{TR}}}\right)\alpha_V\right) \tag{46}$$

$$\frac{\partial^2 \mathcal{F}}{\partial q_i \partial \varepsilon_{kl}} = -VA_{ui}\left(\delta_{kl}\frac{\partial P}{\partial n_u'} + \frac{\partial \varepsilon_{mn}}{\partial n_u'}\mathbb{C}_{\mathrm{T}mnpq}\left(\delta_{pk}\delta_{ql} - \frac{\beta_{\mathrm{T}pq}}{\beta_{\mathrm{TR}}}\delta_{kl}\right)\right) \tag{47}$$

where

$$\frac{\partial \varepsilon_{mn}}{\partial n_u'} = \frac{1}{2}\left(\frac{\partial M_{mp}}{\partial n_u'}M_{np}^{-1} + \frac{\partial M_{np}}{\partial n_u'}M_{mp}^{-1}\right) \tag{48}$$

Appendix D provides a expression for $\partial \boldsymbol{M}/\partial \boldsymbol{n}'$ using the anisotropic equation of state. If the scalar solution equation of state is defined as a function of pressure and temperature (i.e. in terms of the Gibbs energy $\mathcal{G}(P^{\mathcal{G}}, T^{\mathcal{G}}, \boldsymbol{n}^{\mathcal{G}})$), then the following additional conversions are required (Appendix E):

$$\frac{\partial P}{\partial n'_i} = \frac{K_T}{V}\frac{\partial V}{\partial n_i^{\mathcal{G}}} \tag{49}$$

$$\frac{\partial S}{\partial n'_i} = \frac{\partial S}{\partial n_i^{\mathcal{G}}} - \alpha_V K_T \frac{\partial V}{\partial n_i^{\mathcal{G}}} \tag{50}$$

$$\frac{\partial^2 \mathcal{F}}{\partial n'_i \partial n'_j} = \frac{\partial^2 \mathcal{G}}{\partial n_i^{\mathcal{G}} \partial n_j^{\mathcal{G}}} + \frac{\partial V}{\partial n_i^{\mathcal{G}}}\left(\frac{K_T}{V}\right)\frac{\partial V}{\partial n_j^{\mathcal{G}}} \tag{51}$$

3.4 Time-dependent seismic relaxation

If the timescales of relaxation are comparable with the timescales of perturbations in strain, neither unrelaxed properties (Section 3.1) or relaxed properties (Section 3.3) will be able to correctly predict effective material properties. For example, passage of a seismic wave through a material may be too rapid for $\boldsymbol{q}$ to keep pace with the changes in strain at constant entropy. To model time-dependent seismic relaxation, we can assume that relaxation of each structural parameter q_i is driven by the gradient in the internal energy $\mathcal{E}$ with respect to that parameter (analogous to Redfern et al., 1999, replacing the Gibbs energy with the internal energy):

$$\frac{\partial q_i}{\partial t} = -\frac{1}{\lambda_i}\frac{\partial \mathcal{E}}{\partial q_i} \tag{52}$$

In the limit of small strains (and therefore small changes in $\boldsymbol{q}$), the change in internal energy with respect to $\boldsymbol{q}$ can be approximated as linear in $\boldsymbol{\varepsilon}$ and $\boldsymbol{q}$:

$$\frac{\partial q_i}{\partial t} = -\frac{1}{\lambda_i}\left(\frac{\partial^2 \mathcal{E}}{\partial q_i \partial \varepsilon_{jk}}\varepsilon_{jk} + \frac{\partial^2 \mathcal{E}}{\partial q_i \partial q_j}(q_j - q_{j0})\right) \tag{53}$$

This expression can be written as a non-homogeneous linear system of equations with the form

$$\frac{\partial x_i(t)}{\partial t} = A_{ij}x_j(t) + b_i(t) \tag{54}$$

where

$$x_i = q_i - q_{i0} \tag{55}$$

$$A_{ij} = -\frac{1}{\lambda_i}\frac{\partial^2 \mathcal{E}}{\partial q_i \partial q_j} \tag{56}$$

$$b_i(t) = -\frac{1}{\lambda_i}\frac{\partial^2 \mathcal{E}}{\partial q_i \partial \varepsilon_{jk}}\varepsilon_{jk}(t) \tag{57}$$

If there is only one parameter q, the behaviour of q is analogous to the deformation of a forced Kelvin-Voigt body (a viscous dashpot in parallel with a spring). If there are multiple order parameters $\boldsymbol{q}$, the

solution to the non-homogeneous system of equations is (Coddington & Levinson, 1984, p78):

$$\boldsymbol{x} = \exp_{\mathrm{M}}(\boldsymbol{A}(t-t_0))\boldsymbol{x}(t_0) + \int_{t_0}^{t} \exp_{\mathrm{M}}(\boldsymbol{A}(t-s))\boldsymbol{b}(s)ds \tag{58}$$

The steady state response of $\boldsymbol{q}$ to a periodic sinusoidal variation in $\boldsymbol{\varepsilon}$ is a sinusoidal variation with a phase lag. The change in $\boldsymbol{q}$ drives changes in stress and temperature:

$$\Delta\sigma_{ij} = \mathbb{C}_{\mathrm{S}ijkl}\varepsilon_{kl} + \frac{\partial^2\mathcal{E}}{\partial q_k \partial\varepsilon_{ij}}x_k \tag{59}$$

$$\Delta T = \frac{VT}{C_{\boldsymbol{\varepsilon}}}\pi_{kl}\varepsilon_{kl} + \frac{\partial^2\mathcal{E}}{\partial q_k \partial S}x_k \tag{60}$$

where the thermodynamic properties in the above expressions are evaluated at fixed $\boldsymbol{q}$. Analytical expressions for the second order partial derivatives of the internal energy as a function of the partial derivatives of the Helmholtz energy required by Equations 56, 57, 59 and 60 are as follows (Appendix F):

$$\frac{\partial^2\mathcal{E}}{\partial q_i^{\mathcal{E}}\partial S^{\mathcal{E}}} = \frac{T}{C_\varepsilon}\frac{\partial^2\mathcal{F}}{\partial q_i \partial T} \tag{61}$$

$$\frac{\partial^2\mathcal{E}}{\partial q_i^{\mathcal{E}}\partial\varepsilon_{jk}^{\mathcal{E}}} = \frac{\partial^2\mathcal{F}}{\partial q_i \partial\varepsilon_{jk}} + \frac{VT\pi_{jk}}{C_\varepsilon}\frac{\partial^2\mathcal{F}}{\partial q_i \partial T} \tag{62}$$

$$\frac{\partial^2\mathcal{E}}{\partial q_i^{\mathcal{E}}\partial q_j^{\mathcal{E}}} = \frac{\partial^2\mathcal{F}}{\partial q_i \partial q_j} + \frac{\partial^2\mathcal{F}}{\partial q_i \partial T}\frac{T}{C_\varepsilon}\frac{\partial^2\mathcal{F}}{\partial q_j \partial T} \tag{63}$$

4 EXAMPLE: THE STISHOVITE TO POST-STISHOVITE TRANSITION

4.1 Overview

Stishovite is a high-pressure mineral whose composition in natural rocks is close to SiO_2. It is stable in mafic and felsic rocks under the P-T conditions of the mantle transition zone and the upper part of the lower mantle, and has abundances of around 10-25 wt% of rocks with basaltic compositions (Hirose & Fei, 2002; Holland et al., 2013). It has also been identified in meteorites and their shocked target rocks.

Stishovite experiences a symmetry-breaking displacive phase transition with increasing pressure (Kingma et al. 1995; Andrault et al. 1998). This transition involves the rotation of octahedral SiO_6 groups, transforming stishovite from the tetragonal rutile structure (space group $P4_2/mnm$) to the orthorhombic $CaCl_2$ structure (space group Pnnm). The transition takes place at around 50 GPa at room temperature, and around 78 GPa at 2200 K (Fischer et al., 2018), which corresponds to a depth of 1800 km depth along a mantle geotherm (Brown & Shankland, 1981).

At the stishovite to post-stishovite transition, the a- and b-axes of the structure become different lengths. Either the a- or the b- axis can become the longer axis, thus allowing the formation of twins

with $\{110\}$ as a mirror plane. At the transition, the amount of energy and its derivative required to change from post-stishovite ($Q = \delta$) through stishovite ($Q = 0$) to "anti"-post-stishovite ($Q = -\delta$) is zero, and this causes the isothermal or isentropic sum-of-stiffnesses $\mathbb{C}_{11}$ + $\mathbb{C}_{22}$ - 2$\mathbb{C}_{12}$ to drop to zero, and all of the compliances $\mathbb{S}_{11}$, $\mathbb{S}_{22}$ and $\mathbb{S}_{12}$ approaching infinity from both the low and high pressure sides of the transition. In addition, $\mathbb{S}_{13}$ and $\mathbb{S}_{23}$ approach infinity from the high pressure side of the transition.

Several experimental studies have provided data on the stishovite to post-stishovite transition. This includes unit cell data at high pressure (Andrault et al., 2003; Zhang et al., 2023) and high temperature (Ito et al., 1974; Nishihara et al., 2005; Wang et al., 2012; Fischer et al., 2018), and also elastic data at high pressure (Zhang et al., 2021b). These data confirm the qualitative elastic predictions of (Carpenter et al., 2000) which were based on earlier $V(P)$ studies and the frequency decrease of a Raman-active vibrational mode (Kingma et al., 1995).

All the papers modelling the elastic anisotropy of the stishovite to post-stishovite transition (Carpenter et al., 2000; Buchen et al., 2018; Buchen, 2021; Zhang et al., 2021b,a, 2022) have used the athermal Landau formalism introduced by (Carpenter & Salje, 1998). Here, I use a variety of experimental data to parameterise a fully thermal model using the theory described in Sections 2.4 and 3.

4.2 Model formulation

4.2.1 Scalar model

Both stishovite and post-stishovite can be modelled as a solid solution of post-stishovite ($Q = 1$) and anti-post-stishovite ($Q = -1$), where both endmembers have the same properties, but exchanged a and b axes. The high symmetry stishovite structure corresponds to an equimolar mix of these two endmembers.

The displacive second-order transition from stishovite to post-stishovite can be modelled (Carpenter et al., 2000) using a "2-4" Landau-type model, where the "2" and "4" indicate that the excess energy of the solution relative to $\mathcal{G}(Q = 0)$ can be modelled as the sum of a $P-T$ dependent quadratic and constant quartic term in the structure parameter Q. If instead we write the excess energy relative to the energy of the endmembers ($\mathcal{G}(P, T, Q = \pm 1)$), we have:

$$\mathcal{G}_{\text{xs}}(P, T, Q) = (1 - Q^2)(\Delta\mathcal{G}(P, T) + Q^2\Delta\mathcal{G}(P_{\text{tr}}, T_{\text{tr}})), \text{ where} \tag{64}$$

$$\Delta\mathcal{G}(P, T) = \mathcal{G}(P, T, Q = 0) - \mathcal{G}(P, T, Q = 1) \tag{65}$$

The equilibrium value of Q is:

$$Q^* = \begin{cases} 0 \text{ if } \Delta\mathcal{G}(P,T) > \Delta\mathcal{G}(P_{\text{tr}},T_{\text{tr}}) \\ \pm\left(\frac{1}{2}\left(1-\frac{\Delta\mathcal{G}(P,T)}{\Delta\mathcal{G}(P_{\text{tr}},T_{\text{tr}})}\right)\right)^{\frac{1}{2}} \text{ otherwise} \end{cases} \tag{66}$$

The excess Gibbs energy can be rewritten as a function of the proportions of post-stishovite (p_1) and anti-post-stishovite (p_{-1}):

$$\mathcal{G}_{\text{xs}}(P,T,\boldsymbol{p}) = 4p_{-1}p_1\left((\Delta\mathcal{G}(P,T)-\Delta\mathcal{G}(P_{\text{tr}},T_{\text{tr}}))+2\Delta\mathcal{G}(P_{\text{tr}},T_{\text{tr}})(p_{-1}^2+p_1^2)\right) \tag{67}$$

Equation of state parameters (Stixrude & Lithgow-Bertelloni, 2005) for the $Q = 0$ and $Q = 1$ states are fit to the data (Table 3). All parameters apart from the Debye temperature were fit for the $Q = 0$ state, but only the standard state Helmholtz energy, volume and Debye temperature were allowed to differ between the $Q = 1$ and $Q = 0$ members. These three parameters were chosen because they are well constrained by the position and slope of the transition, and on the rate of increase of Q with pressure. The absolute value of Q is somewhat arbitrary, so the Helmholtz energy difference was scaled so that a value of $Q = 1$ lies within the pressure range of the data. The resulting parameters produce a value of $\Delta\mathcal{G}(P_{\text{tr}},T_{\text{tr}}) = -1366$ J/mol. The Gibbs energy as a function of Q at different pressures is shown in Figure 1. The modelled evolution of the equilibrium value of Q is plotted in Figure 2 at a range of pressures and temperatures, and compared with the rotation angle of SiO_6 octahedra about the c-axis from Zhang et al. (2023), which can be used as a proxy for Q.

4.2.2 Anisotropic model

The unrelaxed anisotropic properties of post-stishovite ($Q = 1$) are modelled via a fourth order tensor Ψ (Section 2.4). After some initial investigation, the following formulation was chosen for the elements of the tensor (given in Voigt form):

$$\Psi_{ij}(f,Q=1) = (a_{ij}-(b_1c_1+b_2c_2))f + b_1(\exp(c_1f)-1) + b_2(\exp(c_2f)-1) \tag{68}$$

The available unit cell data at high temperature do not yet support the addition of thermal terms, and there is not yet any elastic tensor data at high temperatures to warrant the use of such terms. The properties of anti-post-stishovite ($Q = -1$) are identical to those of post-stishovite ($Q = 1$), but with the 1st and 2nd rows and columns exchanged, and the 4th and 5th rows and columns exchanged. The Ψ tensor for the solution is treated as linear in Q:

$$\Psi(f,Q) = \left(\frac{1+Q}{2}\right)\Psi(f,Q=1) + \left(\frac{1-Q}{2}\right)\Psi(f,Q=-1) \tag{69}$$

Therefore, the tensor for tetragonal stishovite is given by:

$$\Psi(f,Q=0) = 0.5\left(\Psi(f,Q=1)+\Psi(f,Q=-1)\right) \tag{70}$$

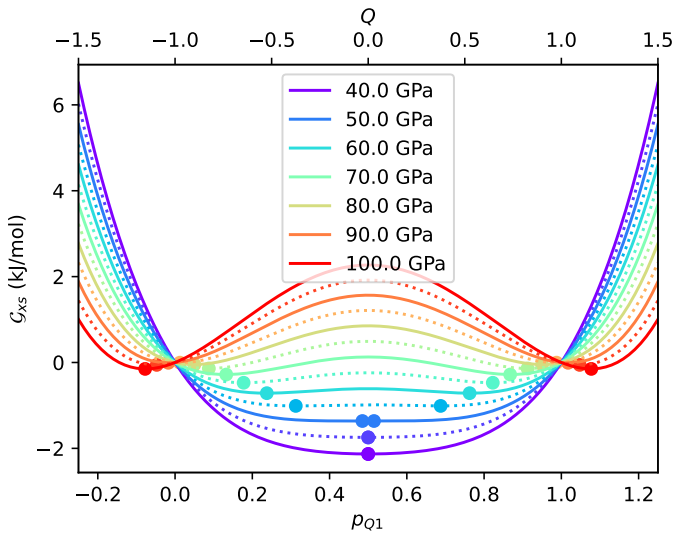

Figure 1. Modelled variation of the excess Gibbs energy relative to post-stishovite with $Q = 1$ at a variety of pressures at 298.15 K. The equilibrium value of the structural parameter Q at each pressure was calculated numerically by minimization of the Gibbs energy and is plotted as a single point (before the symmetry-breaking transition) or two points (after the transition). The transition takes place where $(\partial^2\mathcal{G}/\partial Q\partial Q)_{P,T} = 0$.

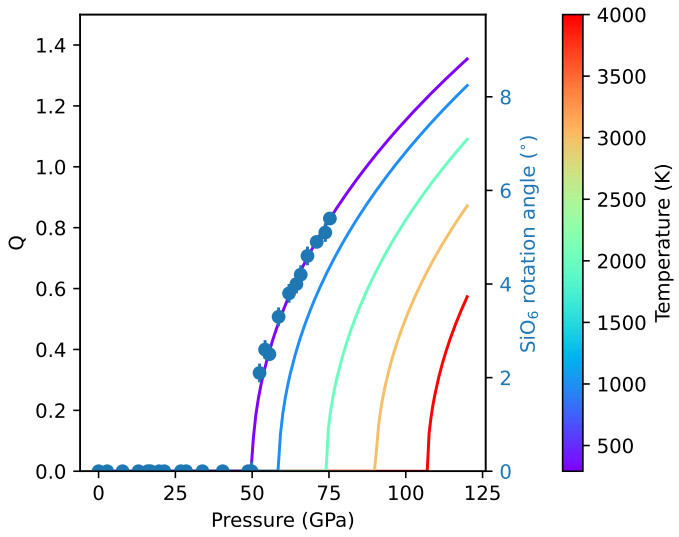

Figure 2. Modelled variation of the equilibrium value of the structural parameter Q in stishovite with respect to pressure and temperature. Values of zero correspond to stishovite, and non-zero values to post-stishovite. Negative values are equally stable, and correspond to "anti"-post-stishovite. Data points correspond to observed SiO_6 rotation angles about the c-axis (Zhang et al., 2023).

To facilitate data inversion, three further functions are defined (for $i = \{1, 2, 3\}$):

$$\Psi_i = \Psi_{i1} + \Psi_{i2} + \Psi_{i3} \tag{71}$$

These parameters can be fit using only the a, b and c unit cell vectors, so these functions facilitate the piece-wise inversion scheme described in Section 4.3. If the diagonal elements of Ψ are also fit to the experimental data, the off-diagonals can be determined by expressions such as:

$$\Psi_{12} = \frac{1}{2}((\Psi_1 + \Psi_2 - \Psi_3) - (\Psi_{11} + \Psi_{22} - \Psi_{33})) \tag{72}$$

4.3 Data processing and inversion

Weighted least squares inversion for the anisotropic properties of stishovite was split into the following stages:

1. Initial fitting of the $\mathcal{G}(P,T)$ equation of state
2. Initial fitting of the unit cell properties $\boldsymbol{M}(V,T,q)$
3. Initial fitting of the relaxed elastic moduli $\mathbb{C}_\mathrm{S}(V,T,q)$
4. Joint inversion of all the experimental data to refine the initial fit parameters.

The initial piece-wise refinement was required to avoid the fitting procedure entering local minima.

4.3.1 Fitting of the $\mathcal{G}(P,T)$ equation of state

In the first step of the inversion, data from six papers were used: $V(P)$ data from Andrault et al. (2003), $V(P)$ and $K_\mathrm{SR}(P)$ data from Zhang et al. (2021b), $V(T)$ data from Ito et al. (1974), $V(P,T)$ data from Nishihara et al. (2005) and Wang et al. (2012) and the transition pressure at 3000 K (taken to be 90 ± 1 GPa) from Fischer et al. (2018). Volumes from Fischer et al. (2018) were not used directly, as they were significantly more scattered than the other datasets.

Some data manipulation was required during fitting to ensure data self-consistency. Firstly, because $1/K_\mathrm{TR} = -(\partial(\ln V)/\partial P)_T$, V(P) data from XRD constrain the isothermal bulk moduli, which at room temperature are closely related to the isentropic moduli obtained from Brillouin and impulsive stimulated light scattering (Kurnosov et al., 2017; Zhang et al., 2021b). Unfortunately, the moduli inferred from the XRD and elasticity data were sufficiently in conflict that hyperparameters were included in the inversion to modify the pressures for each dataset:

$$\frac{P_\mathrm{model}}{P_\mathrm{calibrant}} = a + bP_\mathrm{calibrant} \tag{73}$$

The final values of these hyperparameters after the joint inversion (Section 4.3.4) were $0.8915 + 0.0003P$ (Zhang), $0.9898 - 0.0009P$ (Andrault), $0.9878 - 0.0002P$ (Wang), $0.9957 + 0.0016P$

	$Q=0$	$Q=1$
$\mathcal{F}_0$	-	5.3969e+03
V_0	1.4005e-05	1.3919e-05
K_0	3.0334e+11	as $Q=0$
K_0'	4.0284e+00	as $Q=0$
Debye T_0	1.0922e+03 (SLB)	1.1098e+03
γ_0	1.3480e+00	as $Q=0$
q_0	1.6007e+00	as $Q=0$
a_0	-	2.7278e-02
b_0	-	2.8570e-02

Table 3. Properties of stishovite and post-stishovite as constant structural state as obtained from the available data. a_0 and b_0 are the molar cell lengths at standard pressure and temperature. All properties are given as SI units (J/mol, m^3/mol, Pa, K, m/mol$^{\frac{1}{3}}$). The number of significant digits is not meant to indicate that the values are that well known, but to avoid round-off error. Uncertainties and a correlation matrix of all parameters are provided in Supplementary Information.

(Nishihara), where P is in GPa. Note that only the data of (Zhang et al., 2021a) required significant correction.

Given the very small uncertainties in the reported volumes, the model was interrogated to obtain pressures at the experimentally observed volume and temperature. Pressure uncertainties were chosen to be equal to either the reported uncertainty, or $0.1 + 0.01 \cdot P_{\text{calibrant}}$ [GPa], whichever was the bigger. This downweighted data points with unexpectedly small pressure uncertainties.

Secondly, the room temperature volume of stishovite in the 1 bar study of Ito et al. (1974) was significantly larger than in the studies of Zhang et al. (2021b) and Andrault et al. (2003). Therefore, all the volumes in that study were scaled by a factor $f = V_{0,\,\text{model}}/V_{0,\,\text{Ito}}$, so that the data could still be used to provide an estimate of $(\partial V/\partial T)_P$. Weighted misfits were obtained using the volume uncertainties from the original paper. The optimised parameters obtained from this inversion are given in all except the last two rows of Table 3. The resulting volumes are shown in Figure 3.

4.3.2 Initial fitting of the unit cell properties $\boldsymbol{M}(V,T,q)$

After the initial fitting of the volume and Reuss bulk modulus data, the a, b and c axis lengths were fit using the room temperature stishovite and post-stishovite data from Zhang et al. (2021b) and post-stishovite data from Andrault et al. (2003). Data were fit as a function of pressure, using the modified pressures from Section 4.3.1. The uncertainties in the axis lengths were taken to be equal to either

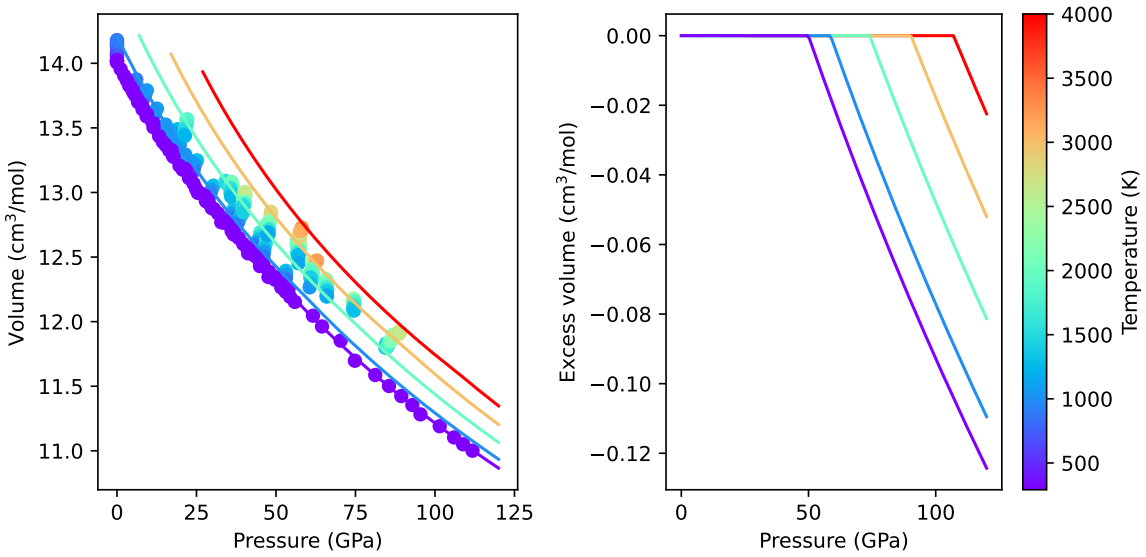

Figure 3. Modelled volume of stishovite to post-stishovite as a function of pressure and temperature. Data points are from the published literature (Ito et al., 1974; Andrault et al., 2003; Fischer et al., 2018; Zhang et al., 2021b). The pressures of the data from Andrault et al. (2003) and Zhang et al. (2021b) are adjusted as described in Section 4.3. Data from Fischer et al. (2018) was not used in the inversion, but is shown for comparison with the model.

the reported uncertainty, or 0.05% of the value of the axis length, whichever was larger. As with the modification to the pressure uncertainties in Section 4.3.1, this downweighted data with unusually small uncertainties.

Data from Ito et al. (1974), Nishihara et al. (2005), Wang et al. (2012) and Fischer et al. (2018) suggests that temperature plays a negligible role in the relative lengths of the a, b and c axes; volume and the structural parameter q have the dominant effect. Furthermore, the length of the c axis appears to be a function only of V (Figure 4). The values optimised during this stage of the inversion are given in the last two rows of Table 3 and the first three rows of Table 4. The resulting evolution of the a, b and c axes is shown in Figure 5.

4.3.3 Initial fitting of the relaxed elastic moduli $\mathbb{C}_S(V, T, q)$

The final data used in the fitting are the elastic moduli from (Zhang et al., 2021b). As for the volume and cell length data, pressures were modified using the hyperparameter values in Section 4.3.1.

Initial attempts at inverting the elasticity data failed to converge on a good solution. The reason for this is that the isentropic compressibility of the three cell axes should be consistent with the corre-

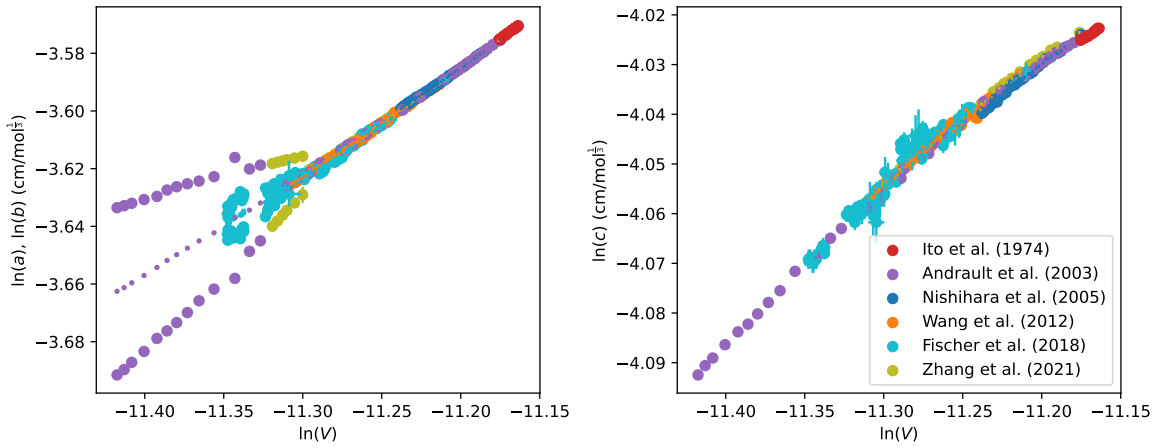

Figure 4. Observed natural logarithm of the a, b and c axis lengths as a function of the natural logarithm of the volume. Data taken from the published literature (Ito et al., 1974; Andrault et al., 2003; Nishihara et al., 2005; Wang et al., 2012; Fischer et al., 2018; Zhang et al., 2021b). The pressures of the high pressure data and the volumes of Ito et al. (1974) are adjusted as described in Section 4.3. Error bars in both x and y are shown, but are mostly smaller than the data points.

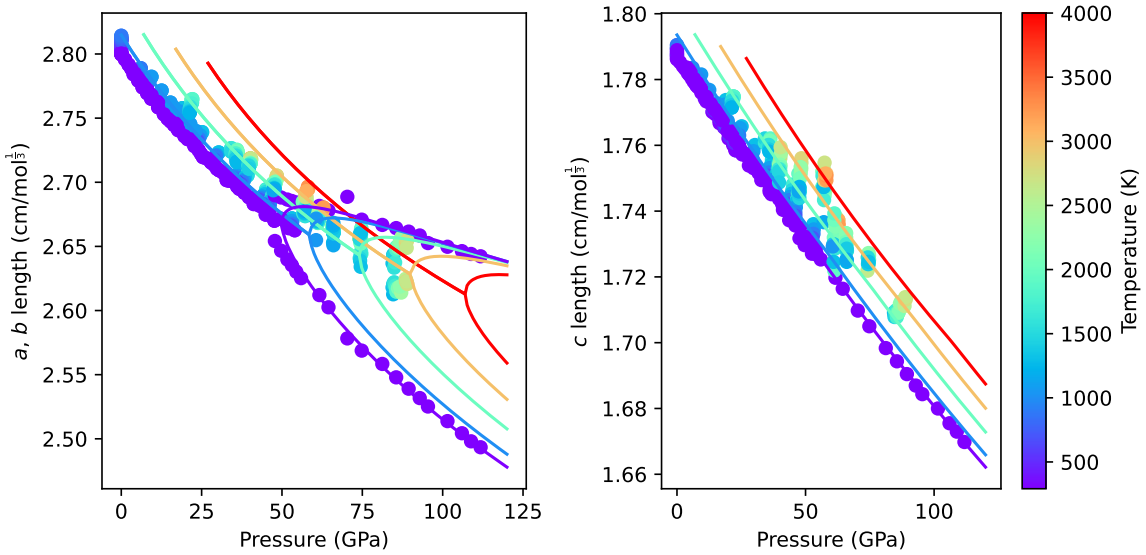

Figure 5. Modelled a, b and c-axis lengths of stishovite to post-stishovite as a function of pressure and temperature. Data points are from the published literature (Ito et al., 1974; Andrault et al., 2003; Nishihara et al., 2005; Wang et al., 2012; Fischer et al., 2018; Zhang et al., 2021b). The pressures of the high pressure data are adjusted as described in Section 4.3.

	a	b_1	c_1	b_2	c_2
Ψ_1	3.9481e-01	3.0141e-01	1.1090e+00	-4.4341e-05	-1.0962e+01
Ψ_2	as above	as above	as above	as above	as above
Ψ_3	2.1039e-01	-6.0281e-01	as above	8.8682e-05	as above
Ψ_{11}	3.2481e-01	8.5214e-01	as above	-1.1294e-02	as above
Ψ_{22}	8.3766e-01	as above	as above	as above	as above
Ψ_{33}	4.9300e-01	-1.4074e-02	as above	-4.1078e-03	as above
Ψ_{44}	1.1196e+00	-2.5749e+00	9.7460e-01	-	-
Ψ_{55}	1.2091e+00	as above	as above	-	-
Ψ_{66}	9.4924e-01	-8.5459e-01	9.9739e-01	-	-

Table 4. Anisotropic parameters for post-stishovite ($Q = 1$). The first three rows correspond to the sum $\Psi_i = \Psi_{i1} + \Psi_{i2} + \Psi_{i3}$. Values in brackets ($\Psi_3$) are not independent - they are uniquely determined by Ψ_1 and Ψ_2. The number of significant digits is not meant to indicate that the values are that well known, but to avoid round-off error. Uncertainties and a correlation matrix of all parameters are provided in Supplementary Information.

sponding components of the compliance tensor:

$$\beta_{\mathrm{S}i} = \mathbb{S}_{\mathrm{S}i1} + \mathbb{S}_{\mathrm{S}i2} + \mathbb{S}_{\mathrm{S}i3} \tag{74}$$

which are found by inverting the elastic stiffness tensor $\mathbb{S}_{\mathrm{S}} = \mathbb{C}_{\mathrm{S}}^{-1}$. The elastic data from Zhang et al. (2021b) indicated a slightly smaller compressibility along the c axis than the unit cell data used in Section 4.3.2. Making the assumption that the Poisson's ratios are less well constrained than the Young's moduli, I modified the off-diagonals of the elastic compliance matrix reported by Zhang et al. (2021b):

$$\mathbb{S}_{\mathrm{S,modified12}} = (\mathbb{S}_{\mathrm{S12}} + (\Delta\beta_{\mathrm{S1}} + \Delta\beta_{\mathrm{S2}} - \Delta\beta_{\mathrm{S3}}/2) \tag{75}$$

$$\mathbb{S}_{\mathrm{S,modified13}} = (\mathbb{S}_{\mathrm{S13}} + (\Delta\beta_{\mathrm{S1}} + \Delta\beta_{\mathrm{S3}} - \Delta\beta_{\mathrm{S2}}/2) \tag{76}$$

$$\mathbb{S}_{\mathrm{S,modified23}} = (\mathbb{S}_{\mathrm{S23}} + (\Delta\beta_{\mathrm{S2}} + \Delta\beta_{\mathrm{S3}} - \Delta\beta_{\mathrm{S1}}/2) \tag{77}$$

$$\Delta\beta_{\mathrm{S}i} = \beta_{\mathrm{S,model}i} - \beta_{\mathrm{S,obs}i} \tag{78}$$

These modified values were then used to calculate a modified stiffness tensor. The differences between the original moduli and the modified moduli are shown in Figure 6 (small data points are the original data, and larger data points are the modified data). Note that the low pressure data are essentially unmodified, with the difference between the original and modified data increasing with increasing pressure.

The misfit was calculated from the difference between this modified stiffness tensor and the model values, weighted by the original uncertainties in the stiffness tensor reported by Zhang et al. (2021b).

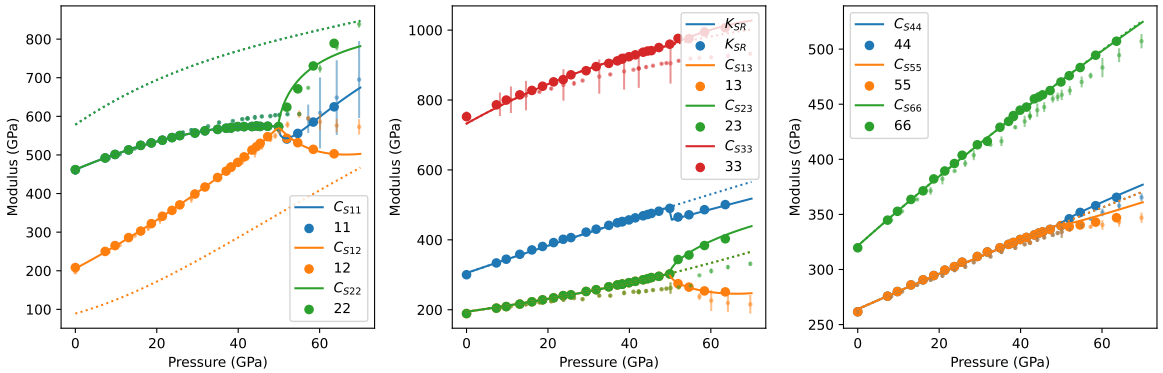

Figure 6. Isentropic elastic stiffness moduli for stishovite and post-stishovite at 298.15 K. Solid lines are the relaxed moduli at the equilibrium value of Q. Dotted lines correspond to the unrelaxed moduli for tetragonal stishovite ($Q = 0$). Small dots are the original from (Zhang et al., 2021b) and large dots correspond to the same moduli pressure- and value-adjusted to satisfy the unit cell constraints from the same paper.

The values optimised during this stage of the inversion are given in the last six rows of Table 4. The resulting elastic stiffness tensor at 298.15 K is shown in Figure 6.

4.3.4 Final joint inversion and model properties

After obtaining an initial set of parameters from the previous steps, all parameters were simultaneously re-optimised using all the experimental data to obtain a global minimum misfit, producing the reported values in Tables 3 and 4 and the hyperparameter values in the text.

The model was then used to calculate the cell tensor and elastic properties as a function of pressure and temperature. The data agree well with the published cell data (Figure 5), including the post-stishovite data from Fischer et al. (2018) that was not used in the inversion. The modeled elastic moduli in Figure 6 are also in very good agreement with the data modified from (Zhang et al., 2021b), suggesting that the formulation of the anisotropic properties contained sufficient parameters to match the experimental data without overfitting.

The model was also used to calculate seismic velocities, linear compressibilities and extrema in Poisson's ratios as a function of crystal orientation just below (Figure 7) and above (Figure 8) the stishovite to post-stishovite transition. As expected, V_{S2} velocities approach zero along the $[1, 1, 0]$ direction from both sides of the transition. Also as expected, the linear compressibility is positive in all directions below the transition - i.e. squeezing stishovite uniaxially results in a smaller volume. In contrast, above the transition, linear compressibility along the longest axis (b) is negative; squeezing the structure uniaxially results in volume expansion. This negative compressibility persists until about 10 GPa above the transition.

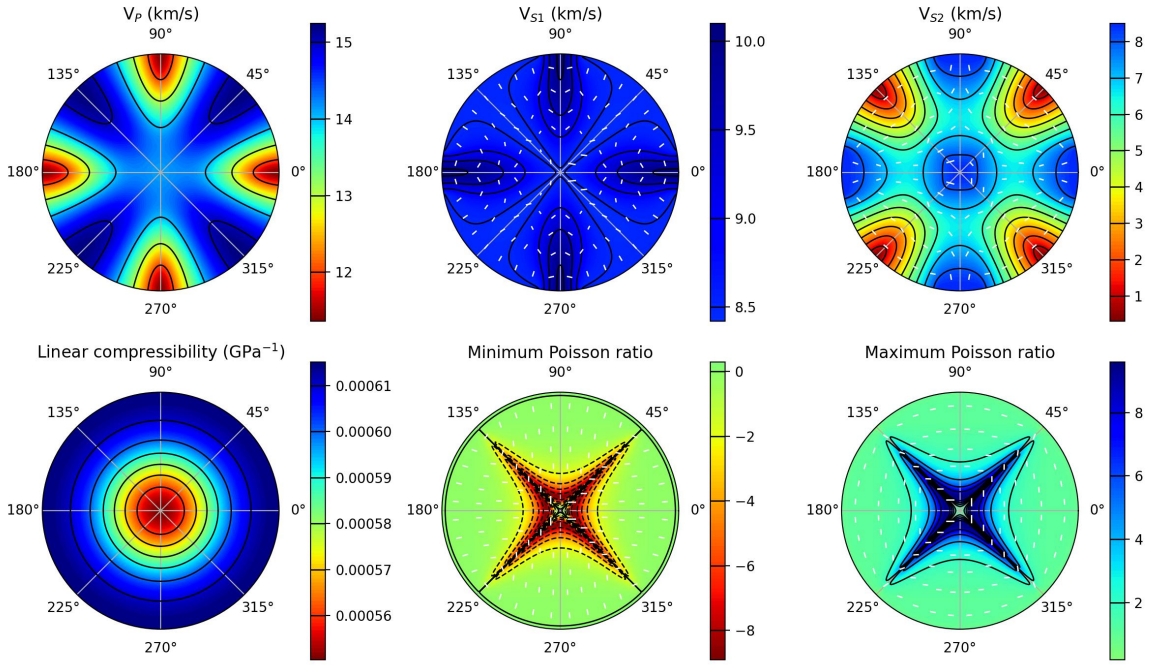

Figure 7. Modelled elastic properties at 77.17 GPa, 2200 K, which is 0.1 GPa lower pressure than the stishovite to post-stishovite transition. Upper hemisphere projection. S-wave velocities are plotted with white lines corresponding to the directions of particle motion. Minimum and maximum Poisson ratios are plotted at positions on the focal sphere that correspond to the axial propagation direction, with white lines corresponding to the lateral directions.

Another interesting observation from the model is that near the transition, the minimum Poisson ratio in almost every direction is negative; that is, when stretched along any direction, crystals of stishovite and post-stishovite also get longer in an orthogonal direction (Figures 7) and 8). This auxetic behaviour decreases in intensity away from the transition. It also becomes more restricted to particular orientations further away from the transition - there are almost no directions of auxeticity 40 GPa below the transition, and auxeticity more than 10 GPa above the transition is restricted to a broad, persistent band surrounding the plane perpendicular to the b axis. A pressure sequence of figures similar to Figures 7) and 8 are provided as Supplementary Materials.

Finally, Figure 9 shows the isotropic velocities V_P, V_Φ, and V_S calculated from the Reuss, Voigt and Voigt-Reuss-Hill (VRH) isentropic bulk and shear moduli. Note the small discontinuity in the VRH compressional and bulk sound velocities at the transition that results from the discontinuous change in the isentropic Reuss bulk modulus. The prominent reduction in V_S associated with the transition has previously been associated with the observation of seismic scatterers in the lower mantle (Kaneshima & Helffrich, 1999; Niu, 2014; Kaneshima, 2019).

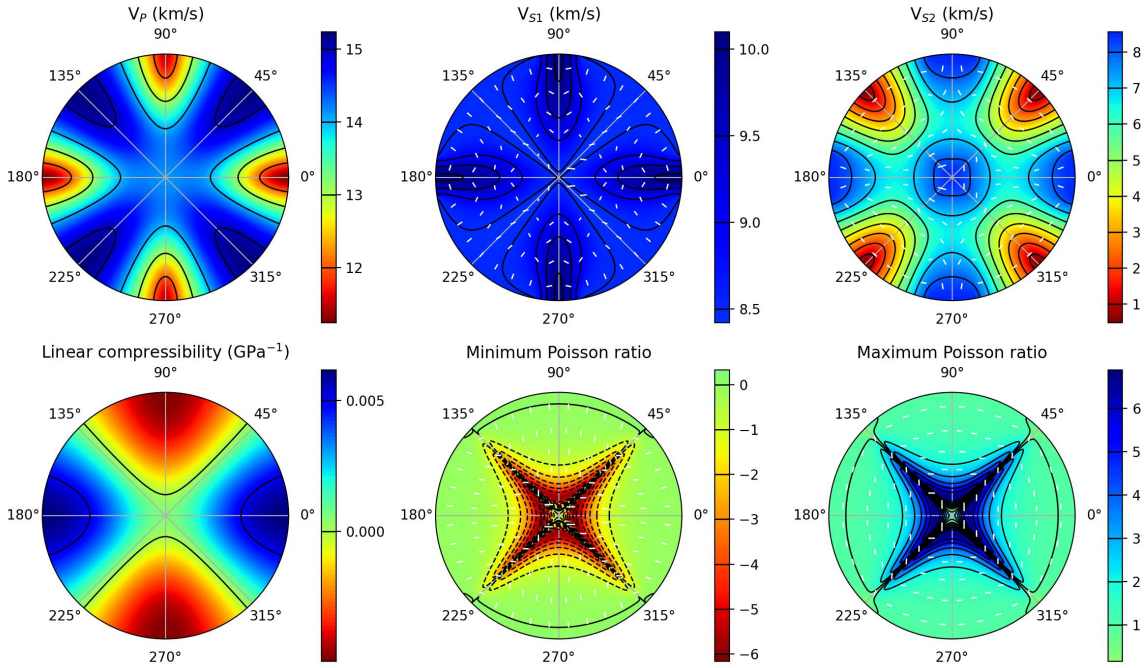

Figure 8. Modelled elastic properties at 77.37 GPa, 2200 K, which is 0.1 GPa higher pressure than the stishovite to post-stishovite transition. Most material properties are similar to Figure 7, with the exception of the linear compressibility. Upper hemisphere projection. S-wave velocities are plotted with white lines corresponding to the directions of particle motion. Minimum and maximum Poisson ratios are plotted at positions on the focal sphere that correspond to the axial propagation direction, with white lines corresponding to the lateral directions.

4.4 The number of optimised parameters

An important test of any predictive model is that it provide a good fit to the available data with the minimum number of parameters. The inversion in this paper involves fitting 37 equation of state parameters. Eight of these are for the scalar model that determines the equilibrium value of q (Table 3). Two further parameters describe the unit cell of post-stishovite at room temperature and pressure (Table 3), seven more describe the evolution of cell parameters at high pressure and temperature, and the other 22 describe the other elastic properties (Table 4).

The number of parameters in this model is somewhat higher than the six scalar parameters (V_0, K_0 and K_0' for both stishovite and post-stishovite) and 21 Landau parameters in the model of (Zhang et al., 2021a). The difference is due in roughly equal parts to the inclusion of thermal terms and a slightly higher expansion order for the elastic tensor. The trade-off is that the model in this paper is thermodynamically consistent, and can be used at high temperature and pressure.

One benefit of the current model is that it can be used to model many different properties simultaneously and self-consistently, and identify conflicts between different kinds of data. Indeed, it

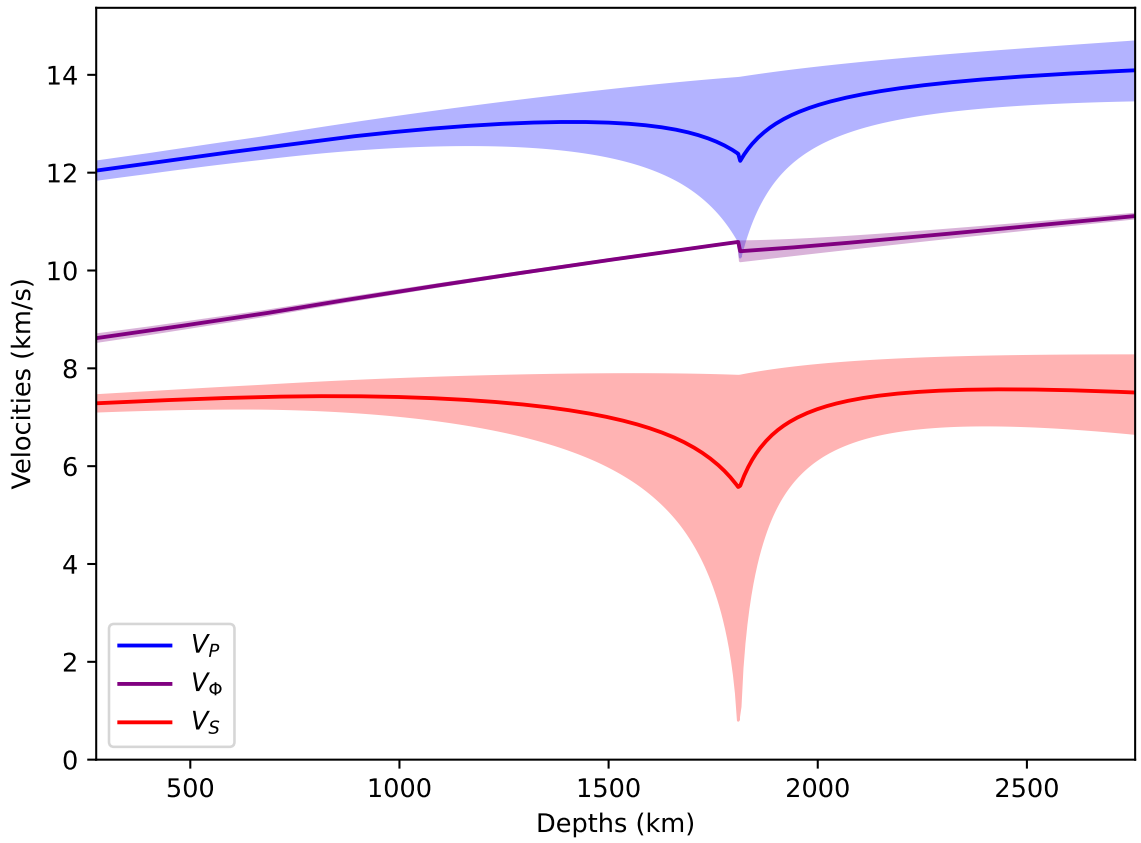

Figure 9. Isotropic seismic velocities of stishovite to post-stishovite along a mantle geotherm (Brown & Shankland, 1981). Shaded regions are bounded by the Reuss and Voigt estimates, solid line represents the Voigt-Reuss-Hill average.

was poor initial fits to the experimental elastic data that led to the identification of discrepancies with available cell data (Section 4.3.3).

5 CONCLUSIONS

The current study shows that it is possible to use the anisotropic solution model of Myhill (2024) to provide quantitative estimates of thermodynamic and elastic properties around second-order displacive phase transitions. Using a comparable number of parameters to existing treatments, the equation of state can be used to calculate all thermodynamic and elastic properties at high temperature and pressure.

The new anisotropic solution model can be built on any traditional scalar model $\mathcal{G}(P,T,\boldsymbol{x})$, thus allowing those interested in elastic properties to use existing datasets. In the context of displacive phase transitions, the method proposed in this paper could be used with existing Bragg & Williams

(1934) or Landau (1935) models that are incorporated into large thermodynamic datasets (Holland & Powell, 2011; Stixrude & Lithgow-Bertelloni, 2024, e.g.,).

Another interesting point to come out of the new treatment is that even when symmetry-breaking strains are relatively large, the anisotropic properties can be accurately reproduced using a linear variation of anisotropic properties (Equation 69). This suggests that extending the method used here to vectors of internal parameters $\boldsymbol{q}$ should be possible without needing unreasonably large sets of model parameters.

ACKNOWLEDGMENTS

Paul Asimow introduced me to seismic relaxation many years ago at the 2014 CIDER workshop. Thanks to him, all the participants, and NSF for providing such a fantastic environment for learning.

Many thanks also to two anonymous reviewers, who provided excellent criticism on an earlier version of this paper.

This work was supported by NERC Large Grant MC-squared (Award No. NE/T012633/1) and STFC (Grant No. ST/R001332/1). Any mistakes or oversights are my own.

DATA AVAILABILITY

The anisotropic equation of state described in this paper is provided as a contribution to the BurnMan open source software project: `https://github.com/geodynamics/burnman` (Cottaar et al., 2014; Myhill et al., 2023).

References

Andrault, D., Angel, R. J., Mosenfelder, J. L., & Le Bihan, T., 2003. Equation of state of stishovite to lower mantle pressures, *American Mineralogist*, **88**(2-3), 301–307.

Angel, R. J., Alvaro, M., Miletich, R., & Nestola, F., 2017. A simple and generalised P–T–V EoS for continuous phase transitions, implemented in EosFit and applied to quartz, *Contributions to Mineralogy and Petrology*, **172**(5).

Antao, S. M., 2016. Quartz: structural and thermodynamic analyses across the α-β transition with origin of negative thermal expansion (nte) in β quartz and calcite, *Acta Crystallographica Section B: Structural Science, Crystal Engineering and Materials*, **72**(2), 249–262.

Bachheimer, J. P. & Dolino, G., 1975. Measurement of the order parameter of α-quartz by second-harmonic generation of light, *Phys. Rev. B*, **11**, 3195–3205.

Bragg, W. L. & Williams, E. J., 1934. The effect of thermal agitation on atomic arrangement in alloys, *Proceedings of the Royal Society of London. Series A, Containing Papers of a Mathematical and Physical Character*, **145**(855), 699–730.

Brown, J. M. & Shankland, T. J., 1981. Thermodynamic parameters in the Earth as determined from seismic profiles, *Geophysical Journal International*, **66**(3), 579–596.

Buchen, J., 2021. *Seismic Wave Velocities in Earth's Mantle from Mineral Elasticity*, chap. 3, pp. 51–95, American Geophysical Union (AGU).

Buchen, J., Marquardt, H., Schulze, K., Speziale, S., Tiziana, Nishiyama, N., & Hanfland, M., 2018. Equation of state of polycrystalline stishovite across the tetragonal-orthorhombic phase transition, *Journal of Geophysical Research: Solid Earth*, **123**(9), 7347–7360.

Cámara, F., Oberti, R., Iezzi, G., & Ventura, G. D., 2003. The P21/m $\longleftrightarrow$ C2/m phase transition in synthetic amphibole $Na(NaMg)Mg_5Si_8O_{22}(OH)_2$: thermodynamic and crystal-chemical evaluation, *Physics and Chemistry of Minerals*, **30**(9), 570–581.

Carpenter, M. A., 2006. Elastic properties of minerals and the influence of phase transitions, *American mineralogist*, **91**(2-3), 229–246.

Carpenter, M. A. & Salje, E. K., 1998. Elastic anomalies in minerals due to structural phase transitions, *European Journal of Mineralogy*, pp. 693–812.

Carpenter, M. A., Salje, E. K., Graeme-Barber, A., Wruck, B., Dove, M. T., & Knight, K. S., 1998. Calibration of excess thermodynamic properties and elastic constant variations associated with the alpha $\longleftrightarrow$ beta phase transition in quartz, *American mineralogist*, **83**(1-2), 2–22.

Carpenter, M. A., Hemley, R. J., & Mao, H.-k., 2000. High-pressure elasticity of stishovite and the P42/mnm–Pnnm phase transition, *Journal of Geophysical Research: Solid Earth*, **105**(B5), 10807–10816.

Coddington, E. A. & Levinson, N., 1984. *Theory of ordinary differential equations*, Tata McGraw-Hill Education, 9th edn.

Cottaar, S., Heister, T., Rose, I., & Unterborn, C., 2014. Burnman: A lower mantle mineral physics toolkit, *Geochemistry, Geophysics, Geosystems*, **15**(4), 1164–1179.

Davies, G. F., 1974. Effective elastic moduli under hydrostatic stress – I. quasi-harmonic theory, *Journal of Physics and Chemistry of Solids*, **35**, 1513–1520.

Devonshire, A., 1949. XCVI. Theory of barium titanate, *The London, Edinburgh, and Dublin Philosophical Magazine and Journal of Science*, **40**(309), 1040–1063.

Dolino, G., 1990. The alpha-inc-beta transitions of quartz: A century of research on displacive phase transitions, *Phase Transitions*, **21**(1), 59–72.

Dove, M. T., 1997. Theory of displacive phase transitions in minerals, *American Mineralogist*, **82**(3-4), 213–244.

Dvořák, V., 1971. The origin of the structural phase transition in $Gd_2(MoO_4)_3$, *physica status solidi (b)*, **45**(1), 147–152.

Fischer, R., Campbell, A., Chidester, B., Reaman, D., Thompson, E. C., Pigott, J., Prakapenka, V., & Smith, J., 2018. Equations of state and phase boundary for stishovite and $CaCl_2$-type SiO_2, *American Mineralogist*, **103**, 792–802.

Ganguly, J., 1982. Mg-Fe order-disorder in ferromagnesian silicates: II. Thermodynamics, kinetics, and geological applications., *Journal of Environmental Sciences (China) English Ed*, pp. 58–99.

Ginzburg, V., 1945. On the dielectric properties of ferroelectric (seignetteelectric) crystals and barium titanate, *Zh. eksp. teor. Fiz*, **15**, 739.

Grønvold, F. & Stølen, S., 1992. Thermodynamics of iron sulfides II. Heat capacity and thermodynamic properties of FeS and of $Fe_{0.875}S$ at temperatures from 298.15 K to 1000 K, of Fe0.98S from 298.15 K to 800 K, and of $Fe_{0.89}S$ from 298.15 K to about 650 K. Thermodynamics of formation, *The Journal of Chemical Thermodynamics*, **24**(9), 913–936.

Heinemann, S., Sharp, T. G., Seifert, F., & Rubie, D. C., 1997. The cubic-tetragonal phase transition in the system majorite ($Mg_4Si_4O_{12}$) - pyrope ($Mg_3Al_2Si_3O_{12}$), and garnet symmetry in the Earth's transition zone, *Physics and Chemistry of Minerals*, **24**(3), 206–221.

Helgeson, H. C., 1978. Summary and critique of the thermodynamic properties of rock-forming minerals, *American Journal of Science*, **278**, 1–229.

Hirose, K. & Fei, Y., 2002. Subsolidus and melting phase relations of basaltic composition in the uppermost lower mantle, *Geochimica et Cosmochimica Acta*, **66**(12), 2099–2108.

Höchli, U., 1972. Elastic constants and soft optical modes in gadolinium molybdate, *Physical Review B*, **6**(5), 1814.

Holland, T. J. B. & Powell, R., 2011. An improved and extended internally consistent thermodynamic dataset for phases of petrological interest, involving a new equation of state for solids, *Journal of Metamorphic Geology*, **29**, 333–383.

Holland, T. J. B., Hudson, N. F. C., Powell, R., & Harte, B., 2013. New Thermodynamic Models and Calculated Phase Equilibria in NCFMAS for Basic and Ultrabasic Compositions through the Transition Zone into the Uppermost Lower Mantle, *Journal of Petrology*, **54**, 1901–1920.

Holzapfel, G., 2000. *Nonlinear Solid Mechanics: A Continuum Approach for Engineering*, John Wiley and Sons, Ltd.

Ito, H., Kawada, K., & Akimoto, S.-i., 1974. Thermal expansion of stishovite, *Physics of the Earth and Planetary Interiors*, **8**(3), 277–281.

Jackson, J. M., Sinogeikin, S. V., Carpenter, M. A., & Bass, J. D., 2004. Novel phase transition in orthoenstatite, *American Mineralogist*, **89**(1), 239–244.

Kaneshima, S., 2019. Seismic scatterers in the lower mantle near subduction zones, *Geophysical Journal International*, **219**(Supplement_1), S2–S20.

Kaneshima, S. & Helffrich, G., 1999. Dipping low-velocity layer in the mid-lower mantle: evidence for geochemical heterogeneity, *Science*, **283**(5409), 1888–1892.

Kimizuka, H., Kaburaki, H., & Kogure, Y., 2003. Molecular-dynamics study of the high-temperature elasticity of quartz above the α-β phase transition, *Physical Review B*, **67**(2), 024105.

Kingma, K. J., Cohen, R. E., Hemley, R. J., & Mao, H.-k., 1995. Transformation of stishovite to a denser phase at lower-mantle pressures, *Nature*, **374**(6519), 243–245.

Kityk, A. V., Schranz, W., Sondergeld, P., Havlik, D., Salje, E. K. H., & Scott, J. F., 2000. Low-frequency superelasticity and nonlinear elastic behavior of $SrTiO_3$, *Physical Review B*, **61**(2), 946–956.

Kurnosov, A., Marquardt, H., Frost, D. J., Ballaran, T. B., & Ziberna, L., 2017. Evidence for a Fe^{3+}-rich pyrolitic lower mantle from (Al,Fe)-bearing bridgmanite elasticity data, *Nature*, **543**, 543–546.

Lacivita, V., D'arco, P., Mustapha, S., Bernardes, D. F., Dovesi, R., Erba, A., & Rérat, M., 2020. Ab initio compressibility of metastable low albite: revealing a lambda-type singularity at pressures of the Earth's upper mantle, *Physics and Chemistry of Minerals*, **47**(10), 1–13.

Lakshtanov, D. L., Sinogeikin, S. V., & Bass, J. D., 2007. High-temperature phase transitions and elasticity of silica polymorphs, *Physics and Chemistry of Minerals*, **34**(1), 11–22.

Landau, L., 1935. Zur Theorie der Anomalien der spezifischen Warme, *Phys. Z. Sowjet*, **8**, 113.

Landau, L., 1937a. Zur Theorie der Phasenum-wandlungen I, *Phys. Z. Sowjet*, **11**, 26.

Landau, L., 1937b. Zur Theorie der Phasenum-wandlungen II, *Phys. Z. Sowjet*, **11**, 545.

Landau, L., 2008. On the Theory of Phase Transitions, *Ukrainian Journal of Physics*, **53**, 25–35.

Landau, L. & Ginzburg, V. L., 1950. On the theory of superconductivity, *JUTP*, **20**, 1064.

Le Chatelier, H., 1890. Sur la dilatation du quartz, *Bulletin de Minéralogie*, **13**(3), 112–118.

Levanyuk, A. & Sannikov, D., 1969. Anomalies in dielectric properties in phase transitions, *Sov Phys JETP*, **28**, 134–139.

Levanyuk, A. & Sannikov, D., 1970. Second order phase transitions close in temperature, *ZhETF Pisma Redaktsiiu*, **11**, 68.

Levanyuk, A. & Sannikov, D., 1971. Phenomenological theory of dielectric anomalies in ferroelectric materials with several phase transitions at temperatures close together, *Sov. Phys. JETP*, **11**, 600–604.

Liakos, J. & Saunders, G., 1982. Application of the Landau theory to elastic phase transitions, *Philosophical Magazine A*, **46**(2), 217–242.

Lüthi, B. & Rehwald, W., 1981. Ultrasonic studies near structural phase transitions, in *Structural Phase Transitions I*, pp. 131–184, eds Müller, K. A. & Thomas, H., Springer Berlin Heidelberg, Berlin, Heidelberg.

Mookherjee, M., Mainprice, D., Maheshwari, K., Heinonen, O., Patel, D., & Hariharan, A., 2016. Pressure induced elastic softening in framework aluminosilicate- albite (NaAlSi3O8), *Scientific Reports*, **6**(1), 34815.

Mueller, H., 1940. Properties of Rochelle Salt, *Phys. Rev.*, **57**, 829–839.

Myhill, R., 2024. An anisotropic equation of state for solid solutions (in prep.), *Geophysical Journal International*.

Myhill, R. & Connolly, J. A., 2021. Notes on the creation and manipulation of solid solution models, *Contributions to Mineralogy and Petrology*, **176**(10), 1–19.

Myhill, R., Cottaar, S., Heister, T., Rose, I., Unterborn, C., Dannberg, J., & Gassmoeller, R., 2023. BurnMan – a Python toolkit for planetary geophysics, geochemistry and thermodynamics, *The Journal of Open Source Software*, **8**(87), 5389.

Nishihara, Y., Nakayama, K., Takahashi, E., Iguchi, T., & Funakoshi, K.-ì., 2005. P-V-T equation of state of stishovite to the mantle transition zone conditions, *Physics and Chemistry of Minerals*, **31**, 660–670.

Niu, F., 2014. Distinct compositional thin layers at mid-mantle depths beneath northeast China revealed by the USArray, *Earth and Planetary Science Letters*, **402**, 305–312.

Nye, J. F. et al., 1985. *Physical properties of crystals: their representation by tensors and matrices*, Oxford University Press.

Powell, R. C., 2010. *Symmetry, Group Theory, and the Physical Properties of Crystals*, vol. 824, Springer.

Redfern, S. A., 1998. Time-temperature-dependent m-site ordering in olivines from high-temperature neutron time-of-flight diffraction, *Physica B: Condensed Matter*, **241-243**, 1189–1196, Proceedings of the International Conference on Neutron Scattering.

Redfern, S. A., Harrison, R. J., O'Neill, H. S., & Wood, D. R., 1999. Thermodynamics and kinetics of cation ordering in $MgAl_2O_4$ spinel up to 1600 °C from in situ neutron diffraction, *American Mineralogist*, **84**(3), 299–310.

Redfern, S. A. T., 2000. Order-Disorder Phase Transitions, *Reviews in Mineralogy and Geochemistry*, **39**(1), 105–133.

Salje, E., 1985. Thermodynamics of sodium feldspar I: order parameter treatment and strain induced coupling effects, *Physics and Chemistry of Minerals*, **12**(2), 93–98.

Seifert, F. A. & Virgo, D., 1975. Kinetics of the Fe^{2+}-Mg, order-disorder reaction in anthophyllites: Quantitative cooling rates, *Science*, **188**(4193), 1107–1109.

Slonczewski, J. C. & Thomas, H., 1970. Interaction of elastic strain with the structural transition of strontium titanate, *Physical Review B*, **1**(9), 3599–3608.

Stixrude, L. & Lithgow-Bertelloni, C., 2005. Thermodynamics of mantle minerals - I. Physical properties, *Geophysical Journal International*, **162**, 610–632.

Stixrude, L. & Lithgow-Bertelloni, C., 2022. Thermal expansivity, heat capacity and bulk modulus of the mantle, *Geophysical Journal International*, **228**(2), 1119–1149.

Stixrude, L. & Lithgow-Bertelloni, C., 2024. Thermodynamics of mantle minerals - III: the role of iron, *Geophysical Journal International*, **237**(3), 1699–1733.

Stixrude, L., Lithgow-Bertelloni, C., Kiefer, B., & Fumagalli, P., 2007. Phase stability and shear softening in $CaSiO_3$ perovskite at high pressure, *Physical Review B*, **75**(2), 024108.

Stokes, H. T. & Hatch, D. M., 1988. *Isotropy Subgroups of the 230 Crystallographic Space Groups*, World Scientific Publishing.

Ter Haar, D., 2013. *Collected papers of LD Landau*, Elsevier.

Thompson, A. & Perkins, E., 1981. Lambda transitions in minerals, in *Thermodynamics of minerals and melts*, pp. 35–62, Springer.

Tröster, A., Schranz, W., & Miletich, R., 2002. How to Couple Landau Theory to an Equation of State, *Phys. Rev. Lett.*, **88**, 055503.

Tröster, A., Schranz, W., Karsai, F., & Blaha, P., 2014. Fully Consistent Finite-Strain Landau Theory for High-Pressure Phase Transitions, *Physical Review X*, **4**(3).

Tröster, A., Ehsan, S., Belbase, K., Blaha, P., Kreisel, J., & Schranz, W., 2017. Finite-strain Landau theory applied to the high-pressure phase transition of lead titanate, *Phys. Rev. B*, **95**, 064111.

Urakawa, S., Someya, K., Terasaki, H., Katsura, T., Yokoshi, S., Funakoshi, K.-i., Utsumi, W., Katayama, Y., Sueda, Y.-i., & Irifune, T., 2004. Phase relationships and equations of state for FeS at high pressures and temperatures and implications for the internal structure of Mars, *Physics of the Earth and Planetary Interiors*, **143**, 469–479.

Wadhawan, V. K., 1982. Ferroelasticity and related properties of crystals, *Phase Transitions*, **3**(1), 3–103.

Wang, F., Tange, Y., Irifune, T., & Funakoshi, K.-i., 2012. P-V-T equation of state of stishovite up to mid-lower mantle conditions, *Journal of Geophysical Research: Solid Earth*, **117**(B6).

Welche, P. R. L., Heine, V., & Dove, M. T., 1998. Negative thermal expansion in beta-quartz, *Physics and Chemistry of Minerals*, **26**(1), 63–77.

Wells, S. A., Dove, M. T., Tucker, M. G., & Trachenko, K., 2002. Real-space rigid-unit-mode analysis of dynamic disorder in quartz, cristobalite and amorphous silica, *Journal of Physics: Condensed Matter*, **14**(18), 4645.

Wu, Z., Justo, J. F., & Wentzcovitch, R. M., 2013. Elastic anomalies in a spin-crossover system: Ferropericlase at lower mantle conditions, *Physical Review Letters*, **110**(22).

Yeganeh-Haeri, A., Weidner, D. J., & Parise, J. B., 1992. Elasticity of α-cristobalite: a silicon dioxide with a negative Poisson's ratio, *Science*, **257**(5070), 650–652.

Zhang, N. B., Cai, Y., Yao, X. H., Zhou, X. M., Li, Y. Y., Song, C. J., Qin, X. Y., & Luo, S. N., 2018. Spin transition of ferropericlase under shock compression, *AIP Advances*, **8**(7), 075028.

Zhang, Y., Chariton, S., He, J., Fu, S., Prakapenka, V. B., & Lin, J.-F., 2021a. Ferroelastic post-stishovite transition mechanism revealed by single-crystal

x-ray diffraction refinements at high pressure, *Earth and Space Science Open Archive*, p. 26.

Zhang, Y., Fu, S., Wang, B., & Lin, J.-F., 2021b. Elasticity of a pseudoproper ferroelastic transition from stishovite to post-stishovite at high pressure, *Phys. Rev. Lett.*, **126**, 025701.

Zhang, Y., Fu, S., Karato, S., Okuchi, T., Chariton, S., Prakapenka, V. B., & Lin, J., 2022. Elasticity of hydrated Al-bearing stishovite and post-stishovite: Implications for understanding regional seismic V_S anomalies along subducting slabs in the lower mantle, *Journal of Geophysical Research: Solid Earth*, **127**(4).

Zhang, Y., Chariton, S., He, J., Fu, S., Xu, F., Prakapenka, V. B., & Lin, J.-F., 2023. Atomistic insight into the ferroelastic post-stishovite transition by high-pressure single-crystal x-ray diffraction, *American Mineralogist*, **108**(1), 110–119.

APPENDIX A: DERIVATION OF THERMODYNAMIC RELATIONS INVOLVING CONJUGATE PROPERTIES

A1 Isentropic and isothermal stiffness tensors

$$d\sigma_{ij} = \left(\frac{\partial \sigma_{ij}}{\partial \varepsilon_{kl}}\right)_T d\varepsilon_{kl} + \left(\frac{\partial \sigma_{ij}}{\partial T}\right)_{\varepsilon_{kl}} dT \tag{A.1}$$

$$dT = \left(\frac{\partial T}{\partial S}\right)_{\varepsilon_{kl}} dS + \left(\frac{\partial T}{\partial \varepsilon_{kl}}\right)_S d\varepsilon_{kl} \tag{A.2}$$

$$= \left(\frac{\partial T}{\partial S}\right)_{\varepsilon_{kl}} dS - \left(\frac{\partial T}{\partial S}\right)_{\varepsilon_{kl}} \left(\frac{\partial S}{\partial \varepsilon_{kl}}\right)_S d\varepsilon_{kl} \tag{A.3}$$

$$= \left(\frac{\partial T}{\partial S}\right)_{\varepsilon_{kl}} dS + \left(\frac{\partial T}{\partial S}\right)_{\varepsilon_{kl}} \left(\frac{\partial \sigma_{kl}}{\partial T}\right)_{\varepsilon_{kl}} d\varepsilon_{kl} \tag{A.4}$$

$$d\sigma_{ij} = \left(\frac{\partial \sigma_{ij}}{\partial \varepsilon_{kl}}\right)_T d\varepsilon_{kl} + \left(\frac{\partial \sigma_{ij}}{\partial T}\right)_{\varepsilon_{kl}} \left(\left(\frac{\partial T}{\partial S}\right)_{\varepsilon_{kl}} dS + \left(\frac{\partial T}{\partial S}\right)_{\varepsilon_{kl}} \left(\frac{\partial \sigma_{kl}}{\partial T}\right)_{\varepsilon_{kl}} d\varepsilon_{kl} \right) \tag{A.5}$$

$$\left(\frac{\partial \sigma_{ij}}{\partial \varepsilon_{kl}}\right)_S = \left(\frac{\partial \sigma_{ij}}{\partial \varepsilon_{kl}}\right)_T + \left(\frac{\partial \sigma_{ij}}{\partial T}\right)_{\varepsilon_{kl}} \left(\frac{\partial T}{\partial S}\right)_{\varepsilon_{kl}} \left(\frac{\partial \sigma_{kl}}{\partial T}\right)_{\varepsilon_{kl}} \tag{A.6}$$

$$V\mathbb{C}_{\mathrm{S}ijkl} = V\mathbb{C}_{\mathrm{T}ijkl} + \frac{T}{C_{\boldsymbol{\varepsilon}}} V\pi_{ij} V\pi_{kl} \tag{A.7}$$

$$\mathbb{C}_{\mathrm{S}ijkl} = \mathbb{C}_{\mathrm{T}ijkl} + \frac{VT}{C_{\boldsymbol{\varepsilon}}} \pi_{ij}\pi_{kl} \tag{A.8}$$

where Equation A.3 uses the triple product rule, Equation A.4 uses the symmetry of double derivatives,

$$\left(\frac{\partial^2 \mathcal{F}}{\partial T \partial \varepsilon_{ij}}\right) = -\left(\frac{\partial S}{\partial \varepsilon_{ij}}\right)_T = \left(\frac{\partial \sigma_{ij}}{\partial T}\right)_{\varepsilon_{kl}} \tag{A.9}$$

and Equation A.6 takes the derivative with respect to strain holding the entropy constant.

A2 Thermal expansivity, isothermal compliance and thermal stress tensors

By the triple product rule:

$$\left(\frac{\partial \varepsilon_{ij}}{\partial T}\right)_{\sigma_{kl}} = -\left(\frac{\partial \varepsilon_{ij}}{\partial \sigma_{kl}}\right)_{T}\left(\frac{\partial \sigma_{kl}}{\partial T}\right)_{\varepsilon_{ij}} \tag{A.10}$$

$$\alpha_{ij} = -\mathbb{S}_{\mathrm{T}ijkl}\pi_{kl} \tag{A.11}$$

A3 Isostress and isostrain heat capacities

$$C_{\boldsymbol{\sigma}} = C_{\boldsymbol{\varepsilon}} + VT\boldsymbol{\alpha}\mathbb{C}_{\mathrm{T}}\boldsymbol{\alpha} \tag{A.12}$$

$$dS = \left(\frac{\partial S}{\partial T}\right)_{\varepsilon_{ij}} dT + \left(\frac{\partial S}{\partial \varepsilon_{ij}}\right)_{T} d\varepsilon_{ij} \tag{A.13}$$

$$= \left(\frac{\partial S}{\partial T}\right)_{\varepsilon_{ij}} dT - \left(\frac{\partial \sigma_{ij}}{\partial T}\right)_{\varepsilon_{pq}} d\varepsilon_{ij} \tag{A.14}$$

$$d\varepsilon_{ij} = \left(\frac{\partial \varepsilon_{ij}}{\partial \sigma_{pq}}\right)_{T} d\sigma_{pq} + \left(\frac{\partial \varepsilon_{ij}}{\partial T}\right)_{\sigma_{pq}} dT \tag{A.15}$$

$$= \left(\frac{\partial \varepsilon_{ij}}{\partial \sigma_{pq}}\right)_{T} d\sigma_{pq} - \left(\frac{\partial \varepsilon_{ij}}{\partial \sigma_{kl}}\right)_{T}\left(\frac{\partial \sigma_{kl}}{\partial T}\right)_{\varepsilon_{pq}} dT \tag{A.16}$$

$$dS = \left(\frac{\partial S}{\partial T}\right)_{\varepsilon_{ij}} dT - \left(\frac{\partial \sigma_{ij}}{\partial T}\right)_{\varepsilon_{ij}}\left(\left(\frac{\partial \varepsilon_{ij}}{\partial \sigma_{pq}}\right)_{T} d\sigma_{pq} - \left(\frac{\partial \varepsilon_{ij}}{\partial \sigma_{kl}}\right)_{T}\left(\frac{\partial \sigma_{kl}}{\partial T}\right)_{\varepsilon_{pq}} dT\right) \tag{A.17}$$

$$\left(\frac{\partial S}{\partial T}\right)_{\sigma_{pq}} = \left(\frac{\partial S}{\partial T}\right)_{\varepsilon_{ij}} + \left(\frac{\partial \sigma_{ij}}{\partial T}\right)_{\varepsilon_{pq}}\left(\frac{\partial \varepsilon_{ij}}{\partial \sigma_{kl}}\right)_{T}\left(\frac{\partial \sigma_{kl}}{\partial T}\right)_{\varepsilon_{pq}} \tag{A.18}$$

$$\frac{1}{T}C_{\boldsymbol{\sigma}} = \frac{1}{T}C_{\boldsymbol{\varepsilon}} + \alpha_{ij}(V\mathbb{C}_{\mathrm{T}ijkl})\alpha_{kl} \tag{A.19}$$

$$C_{\boldsymbol{\sigma}} = C_{\boldsymbol{\varepsilon}} + VT\alpha_{ij}\mathbb{C}_{\mathrm{T}ijkl}\alpha_{kl} \tag{A.20}$$

where Equation A.14 uses the symmetry of double derivatives,

$$\left(\frac{\partial^2 \mathcal{F}}{\partial \varepsilon_{ij}\partial T}\right) = \left(\frac{\partial \sigma_{ij}}{\partial T}\right)_{\varepsilon_{pq}} = -\left(\frac{\partial S}{\partial \varepsilon_{ij}}\right)_{T} \tag{A.21}$$

Equation A.16 uses the triple product rule, and Equation A.18 takes the derivative with respect to temperature holding the stress constant.

APPENDIX B: CALCULATING RELAXED THERMODYNAMIC PROPERTIES

Relaxed thermodynamic properties are determined by minimizing an appropriate thermodynamic potential, allowing some or all isochemical structural variables to vary freely. Similar mathematical

derivations can be used to quantify the effective isotropic thermodynamics of multiphase assemblages by varying the pressure and temperature (Stixrude & Lithgow-Bertelloni, 2022), or consider the anisotropic properties of a single phase, as we do here.

Let us seek expressions for the relaxed second order derivatives of the Helmholtz energy. We first define a set of functions $P_l(\boldsymbol{M}, T, \boldsymbol{q})$ that describe the partial derivatives of the Helmholtz energy with respect to $\boldsymbol{q}$:

$$P_l(\boldsymbol{M}, T, \boldsymbol{q}) = \frac{\partial \mathcal{F}}{\partial q_l} \tag{B.1}$$

where $\boldsymbol{M}$ is the extensive metric tensor, with elements having units of m, and $\boldsymbol{q}$ are the unitless isochemical structural vectors. The minimization of $\mathcal{F}$ is achieved when

$$P_l(\boldsymbol{M}, T, \boldsymbol{q}^*(\boldsymbol{M}, T)) = 0_l \tag{B.2}$$

The relaxed properties $\mathbb{C}_\mathrm{T}^*$, $\boldsymbol{\pi}^*$ and c_ε^* depend on the way in which $\boldsymbol{q}^*$ varies due to small changes in $\boldsymbol{\varepsilon}$ or T (here collected as $\boldsymbol{z} = \{\boldsymbol{\varepsilon}, T\}$). This dependence can be determined by applying the chain rule:

$$\frac{\partial P_l}{\partial z_j} + \frac{\partial P_l}{\partial q_m^*}\frac{\partial q_m^*}{\partial z_j} = 0_{lj} \tag{B.3}$$

and solving for $\partial q_m^*/z_j$:

$$\frac{\partial P_l}{\partial q_m}\frac{\partial q_m^*}{\partial z_j} = -\frac{\partial P_l}{\partial z_j} \tag{B.4}$$

$$R_{kl}\frac{\partial P_l}{\partial q_m}\frac{\partial q_m^*}{\partial z_j} = -R_{kl}\frac{\partial P_l}{\partial z_j} \tag{B.5}$$

$$\frac{\partial q_k^*}{\partial z_j} = -R_{kl}\frac{\partial P_l}{\partial z_j} \tag{B.6}$$

where R is the left inverse matrix:

$$\delta_{km} = R_{kl}\frac{\partial P_l}{\partial q_m} \tag{B.7}$$

$$= R_{kl}\frac{\partial^2 \mathcal{F}}{\partial q_l \partial q_m} \tag{B.8}$$

The relaxed physical properties evaluated at constant T are then determined by repeated application of the chain rule:

$$\frac{\partial \mathcal{F}^*}{\partial z_i} = \frac{\partial \mathcal{F}}{\partial z_i} + \frac{\partial \mathcal{F}}{\partial q_k}\frac{\partial q_k^*}{\partial z_i} \tag{B.9}$$

$$= \frac{\partial \mathcal{F}}{\partial z_i} \tag{B.10}$$

where the second term in the first expression vanished by the requirement that $\partial \mathcal{F}/\partial q_k = 0_k$ at

equilibrium (Equation B.2). Differentiating again yields

$$\frac{\partial^2 \mathcal{F}^*}{\partial z_i \partial z_j} = \frac{\partial^2 \mathcal{F}}{\partial z_i \partial z_j} + \frac{\partial^2 \mathcal{F}}{\partial z_i \partial q_k} \frac{\partial q_k^*}{\partial z_j} \tag{B.11}$$

$$= \frac{\partial^2 \mathcal{F}}{\partial z_i \partial z_j} - \frac{\partial^2 \mathcal{F}}{\partial z_i \partial q_k} R_{kl} \frac{\partial^2 \mathcal{F}}{\partial q_l \partial z_j} \tag{B.12}$$

$$\left[\begin{array}{c|c} V\mathbb{C}_{\mathrm{T}}^* & V\boldsymbol{\pi}^* \\ \hline V\boldsymbol{\pi}^{*\mathrm{T}} & -C_{\boldsymbol{\varepsilon}}^*/T \end{array}\right]_{ij} = \left[\begin{array}{c|c} V\mathbb{C}_{\mathrm{T}} & V\boldsymbol{\pi} \\ \hline V\boldsymbol{\pi}^{\mathrm{T}} & -C_{\boldsymbol{\varepsilon}}/T \end{array}\right]_{ij} - \frac{\partial^2 \mathcal{F}}{\partial z_i \partial q_k} R_{kl} \frac{\partial^2 \mathcal{F}}{\partial q_l \partial z_j} \tag{B.13}$$

This expression is similar to the expression under fixed entropy constraints presented by Slonczewski & Thomas (1970), their Equation 26. The elements of the unrelaxed block matrix (first term on the RHS of the last equation) can be evaluated directly from the anisotropic equation of state. Expressions for $\partial^2 \mathcal{F}/\partial \boldsymbol{q} \partial \boldsymbol{q}$ (Equation B.8) and $\partial^2 \mathcal{F}/\partial \boldsymbol{q} \partial \boldsymbol{z}$ (Equation B.13) can be derived by change of variables (Appendix C).

APPENDIX C: CHANGE OF VARIABLES AND DERIVATIVES OF THE HELMHOLTZ ENERGY

Here, we derive the partial derivatives in Section 3.3.2 by change of variables. The variables required are:

$$\left(\frac{\partial^2 \mathcal{F}}{\partial q_i \partial q_j}\right)_{\boldsymbol{M}_{\mathrm{ref}}, \boldsymbol{\varepsilon}, T, q_{k\neq i, k\neq j}, \boldsymbol{x}}, \left(\frac{\partial^2 \mathcal{F}}{\partial q_i \partial T}\right)_{\boldsymbol{M}_{\mathrm{ref}}, \boldsymbol{\varepsilon}, \boldsymbol{q}_{j\neq i}, \boldsymbol{x}}, \left(\frac{\partial^2 \mathcal{F}}{\partial q_i \partial \varepsilon_{kl}}\right)_{\boldsymbol{M}_{\mathrm{ref}}, \boldsymbol{\varepsilon}_{mn\neq kl}, T, q_{j\neq i}, \boldsymbol{x}} \tag{C.1}$$

where $\boldsymbol{M}_{\mathrm{ref}}$ is a constant reference cell tensor about which small strains can be performed. The equation of state developed by Myhill (2024) gives the partial derivatives of $\mathcal{F}(f', T', \boldsymbol{n}', \bar{\boldsymbol{\varepsilon}}')$, where $f = \ln V$. The "primes" are used to specify the variables of the equation of state. Making explicit the dependences on the variables in C.1, we have:

$$\mathcal{F} = \mathcal{F}(f'(\boldsymbol{M}_{\mathrm{ref}}, \boldsymbol{\varepsilon}), T'(T), \boldsymbol{n}'(\boldsymbol{q}, \boldsymbol{x}), \bar{\boldsymbol{\varepsilon}}'(\boldsymbol{M}_{\mathrm{ref}}, \boldsymbol{\varepsilon}, T, \boldsymbol{q}, \boldsymbol{x}))$$

The partial differential operators for the set of variables in C.1 are thus:

$$\frac{\partial}{\partial q_i} = \frac{\partial n'_u}{\partial q_i} \frac{\partial}{\partial n'_u} + \frac{\partial \bar{\varepsilon}'_{mn}}{\partial q_i} \frac{\partial}{\partial \bar{\varepsilon}'_{mn}} \tag{C.2}$$

$$\frac{\partial}{\partial T} = \frac{\partial}{\partial T'} + \frac{\partial \bar{\varepsilon}'_{pq}}{\partial T} \frac{\partial}{\partial \bar{\varepsilon}'_{pq}} \tag{C.3}$$

$$\frac{\partial}{\partial \varepsilon_{kl}} = \frac{\partial f'}{\partial \varepsilon_{kl}} \frac{\partial}{\partial f'} + \frac{\partial \bar{\varepsilon}'_{pq}}{\partial \varepsilon_{kl}} \frac{\partial}{\partial \bar{\varepsilon}'_{pq}} \tag{C.4}$$

In order to write the second derivatives in their most compact form, we first need to derive some of the partial derivatives in the three expressions above. These are:

- The constant stoichiometric ordering matrix:

$$\frac{\partial n'_i}{\partial q_j} = A_{ij} \tag{C.5}$$

- The small strain identity:

$$\frac{\partial f'}{\partial \varepsilon_{ij}} = \delta_{ij} \tag{C.6}$$

- Other derivatives are calculated considering the total derivative of the small strain tensor $\boldsymbol{\varepsilon}$:

$$d\varepsilon_{ij} = \frac{\partial \varepsilon_{ij}}{\partial f'} df' + \frac{\partial \varepsilon_{ij}}{\partial T'} dT' + \frac{\partial \varepsilon_{ij}}{\partial n'_k} dn'_k + \frac{\partial \varepsilon_{ij}}{\partial \bar{\varepsilon}'_{lm}} d\bar{\varepsilon}'_{lm} \tag{C.7}$$

- Taking the partial derivative with respect to ε_{kl} at constant T, $\boldsymbol{q}$ and $\boldsymbol{x}$:

$$\frac{\partial \bar{\varepsilon}'_{ij}}{\partial \varepsilon_{kl}} = \frac{\partial \varepsilon_{ij}}{\partial \varepsilon_{kl}} - \frac{\partial \varepsilon_{ij}}{\partial f'} \frac{\partial f'}{\partial \varepsilon_{kl}} = \delta_{ik}\delta_{jl} - \frac{\beta_{\mathrm{T}ij}}{\beta_{\mathrm{TR}}} \delta_{kl} \tag{C.8}$$

- with respect to q_i at constant $\boldsymbol{\varepsilon}$ $(= 0)$, T and $\boldsymbol{x}$:

$$\frac{\partial \bar{\varepsilon}'_{mn}}{\partial q_i} = -\frac{\partial \varepsilon_{mn}}{\partial n'_u} \frac{\partial n'_u}{\partial q_i} = -\frac{\partial \varepsilon_{mn}}{\partial n'_u} A_{ui} \tag{C.9}$$

- with respect to T at constant $\boldsymbol{\varepsilon}$ $(= 0)$, $\boldsymbol{q}$ and $\boldsymbol{x}$:

$$\frac{\partial \bar{\varepsilon}'_{mn}}{\partial T} = -\frac{\partial \varepsilon_{mn}}{\partial T'} = -\left(\frac{\alpha_{ij}}{\alpha_V} - \frac{\beta_{\mathrm{T}ij}}{\beta_{\mathrm{TR}}} \right) \alpha_V \tag{C.10}$$

- Assuming a hydrostatic reference state, we also have:

$$\frac{\partial \sigma_{ij}}{\partial X'} = -\delta_{ij} \frac{\partial P}{\partial X'} \text{ where } X \text{ could be } f', T' \text{ or } \boldsymbol{n}'. \tag{C.11}$$

$$\delta_{ij} \frac{\partial \varepsilon_{ij}}{\partial X'} = 0 \text{ where } X \text{ could be } T', \boldsymbol{n}' \text{ or } \bar{\boldsymbol{\varepsilon}}'. \tag{C.12}$$

Using these expressions, we can compactly write the second derivatives of interest:

$$\frac{\partial^2 \mathcal{F}}{\partial q_i \partial q_j} = \frac{\partial n'_u}{\partial q_i} \frac{\partial}{\partial n'_u} \left(\frac{\partial n'_v}{\partial q_j} \frac{\partial \mathcal{F}}{\partial n'_v} + \frac{\partial \bar{\varepsilon}'_{mn}}{\partial q_j} \frac{\partial \mathcal{F}}{\partial \bar{\varepsilon}'_{mn}} \right) + \frac{\partial \bar{\varepsilon}'_{mn}}{\partial q_i} \frac{\partial}{\partial \bar{\varepsilon}'_{mn}} \left(\frac{\partial n'_u}{\partial q_j} \frac{\partial \mathcal{F}}{\partial n'_u} + \frac{\partial \bar{\varepsilon}'_{pq}}{\partial q_j} \frac{\partial \mathcal{F}}{\partial \bar{\varepsilon}'_{pq}} \right) \tag{C.13}$$

$$= \frac{\partial n'_u}{\partial q_i} \left(\frac{\partial n'_v}{\partial q_j} \frac{\partial^2 \mathcal{F}}{\partial n'_u \partial n'_v} + \frac{\partial \bar{\varepsilon}'_{mn}}{\partial q_j} \frac{\partial^2 \mathcal{F}}{\partial n'_u \partial \bar{\varepsilon}'_{mn}} \right) + \frac{\partial \bar{\varepsilon}'_{mn}}{\partial q_i} \left(\frac{\partial n'_u}{\partial q_j} \frac{\partial^2 \mathcal{F}}{\partial n'_u \partial \bar{\varepsilon}'_{mn}} + \frac{\partial \bar{\varepsilon}'_{pq}}{\partial q_j} \frac{\partial^2 \mathcal{F}}{\partial \bar{\varepsilon}'_{pq} \partial \bar{\varepsilon}'_{mn}} \right) \tag{C.14}$$

$$= A_{ui} \left(A_{vj} H^{\mathcal{F}}_{uv} + \frac{\partial \bar{\varepsilon}'_{mn}}{\partial q_j} \frac{\partial \sigma_{mn}}{\partial n'_u} \right) + \frac{\partial \bar{\varepsilon}'_{mn}}{\partial q_i} \left(A_{uj} \frac{\partial \sigma_{mn}}{\partial n'_u} + \frac{\partial \bar{\varepsilon}'_{pq}}{\partial q_j} V \mathbb{C}_{\mathrm{T}mnpq} \right) \tag{C.15}$$

$$= A_{ui} \left(A_{vj} H^{\mathcal{F}}_{uv} + \frac{\partial \varepsilon_{mn}}{\partial n'_v} A_{vj} \delta_{mn} \frac{\partial P}{\partial n'_u} \right) - \frac{\partial \varepsilon_{mn}}{\partial n'_u} A_{ui} \left(-A_{vj} \delta_{mn} \frac{\partial P}{\partial n'_v} - \frac{\partial \varepsilon_{pq}}{\partial n'_v} A_{vj} V \mathbb{C}_{\mathrm{T}mnpq} \right) \tag{C.16}$$

$$= A_{ui} \left(H^{\mathcal{F}}_{uv} + V \frac{\partial \varepsilon_{mn}}{\partial n'_u} \mathbb{C}_{\mathrm{T}mnpq} \frac{\partial \varepsilon_{pq}}{\partial n'_v} \right) A_{vj} \tag{C.17}$$

$$\frac{\partial^2 \mathcal{F}}{\partial q_i \partial T} = \frac{\partial}{\partial T'}\left(\frac{\partial n'_u}{\partial q_i}\frac{\partial \mathcal{F}}{\partial n'_u} + \frac{\partial \bar{\varepsilon}'_{mn}}{\partial q_i}\frac{\partial \mathcal{F}}{\partial \bar{\varepsilon}'_{mn}}\right) + \frac{\partial \bar{\varepsilon}'_{pq}}{\partial T}\frac{\partial}{\partial \bar{\varepsilon}'_{pq}}\left(\frac{\partial n'_u}{\partial q_i}\frac{\partial \mathcal{F}}{\partial n'_u} + \frac{\partial \bar{\varepsilon}'_{mn}}{\partial q_i}\frac{\partial \mathcal{F}}{\partial \bar{\varepsilon}'_{mn}}\right) \tag{C.18}$$

$$= \left(\frac{\partial n'_u}{\partial q_i}\frac{\partial^2 \mathcal{F}}{\partial n'_u \partial T'} + \frac{\partial \bar{\varepsilon}'_{mn}}{\partial q_i}\frac{\partial^2 \mathcal{F}}{\partial \bar{\varepsilon}'_{mn}\partial T'}\right) + \frac{\partial \bar{\varepsilon}'_{pq}}{\partial T}\left(\frac{\partial n'_u}{\partial q_i}\frac{\partial^2 \mathcal{F}}{\partial n'_u \partial \bar{\varepsilon}'_{pq}} + \frac{\partial \bar{\varepsilon}'_{mn}}{\partial q_i}\frac{\partial^2 \mathcal{F}}{\partial \bar{\varepsilon}'_{mn}\partial \bar{\varepsilon}'_{pq}}\right) \tag{C.19}$$

$$= \left(-A_{ui}\frac{\partial S}{\partial n'_u} - \frac{\partial \varepsilon_{mn}}{\partial n'_i}A_{ui}V\frac{\partial \sigma_{mn}}{\partial T'}\right) - \frac{\partial \varepsilon_{pq}}{\partial T'}\left(A_{ui}V\frac{\partial \sigma_{pq}}{\partial n'_u} - \frac{\partial \bar{\varepsilon}'_{mn}}{\partial n'_u}A_{ui}V\mathbb{C}_{\mathrm{T}mnpq}\right) \tag{C.20}$$

$$= A_{ui}\left(-\frac{\partial S}{\partial n'_u} + V\frac{\partial \varepsilon_{mn}}{\partial n'_u}\mathbb{C}_{\mathrm{T}mnpq}\left(\frac{\alpha_{pq}}{\alpha_V} - \frac{\beta_{\mathrm{T}pq}}{\beta_{\mathrm{TR}}}\right)\alpha_V\right) \tag{C.21}$$

$$\frac{\partial^2 \mathcal{F}}{\partial q_i \partial \varepsilon_{kl}} = \frac{\partial f'}{\partial \varepsilon_{kl}}\frac{\partial}{\partial f'}\left(\frac{\partial n'_u}{\partial q_i}\frac{\partial \mathcal{F}}{\partial n'_u} + \frac{\partial \bar{\varepsilon}'_{mn}}{\partial q_i}\frac{\partial \mathcal{F}}{\partial \bar{\varepsilon}'_{mn}}\right) + \frac{\partial \bar{\varepsilon}'_{pq}}{\partial \varepsilon_{kl}}\frac{\partial}{\partial \bar{\varepsilon}'_{pq}}\left(\frac{\partial n'_u}{\partial q_i}\frac{\partial \mathcal{F}}{\partial n'_u} + \frac{\partial \bar{\varepsilon}'_{mn}}{\partial q_i}\frac{\partial \mathcal{F}}{\partial \bar{\varepsilon}'_{mn}}\right) \tag{C.22}$$

$$= \frac{\partial f'}{\partial \varepsilon_{kl}}\left(\frac{\partial n'_u}{\partial q_i}\frac{\partial^2 \mathcal{F}}{\partial n'_u \partial f'} + \frac{\partial \bar{\varepsilon}'_{mn}}{\partial q_i}\frac{\partial^2 \mathcal{F}}{\partial \bar{\varepsilon}'_{mn}\partial f'}\right) + \frac{\partial \bar{\varepsilon}'_{pq}}{\partial \varepsilon_{kl}}\left(\frac{\partial n'_u}{\partial q_i}\frac{\partial^2 \mathcal{F}}{\partial n'_u \partial \bar{\varepsilon}'_{pq}} + \frac{\partial \bar{\varepsilon}'_{mn}}{\partial q_i}\frac{\partial^2 \mathcal{F}}{\partial \bar{\varepsilon}'_{mn}\partial \bar{\varepsilon}'_{pq}}\right) \tag{C.23}$$

$$= A_{ui}\left(\delta_{kl}\left(-V\frac{\partial P}{\partial n'_u} - \frac{\partial \varepsilon_{mn}}{\partial n'_u}V\frac{\partial \sigma_{mn}}{\partial f'}\right) + \frac{\partial \bar{\varepsilon}'_{pq}}{\partial \varepsilon_{kl}}\left(V\frac{\partial \sigma_{pq}}{\partial n'_u} - \frac{\partial \varepsilon_{mn}}{\partial n'_u}V\mathbb{C}_{\mathrm{T}mnpq}\right)\right) \tag{C.24}$$

$$= -VA_{ui}\left(\delta_{kl}\frac{\partial P}{\partial n'_u} + \frac{\partial \varepsilon_{mn}}{\partial n'_u}\mathbb{C}_{\mathrm{T}mnpq}\left(\delta_{pk}\delta_{ql} - \frac{\beta_{\mathrm{T}pq}}{\beta_{\mathrm{TR}}}\delta_{kl}\right)\right) \tag{C.25}$$

APPENDIX D: CHANGE OF VARIABLES: COMPOSITIONAL DERIVATIVE OF THE CELL TENSOR

This appendix provides the first compositional derivative of the cell tensor under hydrostatic conditions $\boldsymbol{M}(V_{\mathrm{mol}}(V^\circ, \boldsymbol{n}^\circ), T(T^\circ), \boldsymbol{p}(\boldsymbol{n}^\circ), n(\boldsymbol{n}^\circ))$, where $^\circ$ denotes the required variable set:

$$\boldsymbol{M} = \boldsymbol{F}\boldsymbol{M}_0 \tag{D.1}$$

$$\ln_{\mathrm{M}} \boldsymbol{M}_0(\boldsymbol{p}, n) = p_m(\ln_{\mathrm{M}}(\boldsymbol{M}_{0m})) + \frac{\ln(n)}{3}\boldsymbol{I} \tag{D.2}$$

$$\ln_{\mathrm{M}} \boldsymbol{F}(V_{\mathrm{mol}}, T, \boldsymbol{p}) = (p_m \Psi_{ijklm}(V_{\mathrm{mol}}, T) + p_m p_n \mathbb{W}^{\Psi}_{ijklmn}(V_{\mathrm{mol}}, T, \boldsymbol{p}))\delta_{kl} \tag{D.3}$$

$$\text{where } V_{\mathrm{mol}} = \frac{V}{n},\ p_m = \frac{n_m}{n}, \text{ and } n = 1_l n_l \tag{D.4}$$

$$\text{so } \frac{\partial V_{\mathrm{mol}}}{\partial n^\circ_l} = -\frac{1_l V_{\mathrm{mol}}}{n},\ \frac{\partial n}{\partial n^\circ_l} = 1_l, \text{ and } = \frac{\partial p_m}{\partial n^\circ_l} = \left(\frac{n\delta_{lm} - 1_l n_m}{n^2}\right) = \left(\frac{\delta_{lm} - 1_l p_m}{n}\right) \tag{D.5}$$

Additionally, because $\boldsymbol{M_0 I} = \boldsymbol{I M_0}$, we can write

$$\frac{\partial M_{0kj}}{\partial n} = \frac{M_{0kj}}{3n^{2/3}}, \text{ and } \frac{\partial M_{0kj}}{\partial p_m} = n^{1/3}\frac{\partial M_{0\mathrm{mol}kj}}{\partial p_m} \tag{D.6}$$

$$\frac{\partial M_{ij}}{\partial n_l^\circ} = \frac{\partial F_{ik}}{\partial n_l^\circ} M_{0kj} + F_{ik} \frac{\partial M_{0kj}}{\partial n_l^\circ} \tag{D.7}$$

$$\frac{\partial F_{ik}}{\partial n_l^\circ} = \frac{\partial F_{ik}}{\partial V_{\text{mol}}} \frac{\partial V_{\text{mol}}}{\partial n_l^\circ} + \frac{\partial F_{ik}}{\partial p_m} \frac{\partial p_m}{\partial n_l^\circ} \tag{D.8}$$

$$= -\frac{\partial F_{ik}}{\partial V_{\text{mol}}} \frac{1_l V_{\text{mol}}}{n} + \frac{\partial F_{ik}}{\partial p_m} \left(\frac{\delta_{lm} - 1_l p_m}{n} \right) \tag{D.9}$$

$$\frac{\partial M_{0kj}}{\partial n_l^\circ} = \frac{\partial M_{0kj}}{\partial n} \frac{\partial n}{\partial n_l^\circ} + \frac{\partial M_{0kj}}{\partial p_m} \frac{\partial p_m}{\partial n_l^\circ} \tag{D.10}$$

$$= \frac{M_{0kj}}{3n^{2/3}} 1_l + \frac{\partial M_{0\text{mol}kj}}{\partial p_m} \left(\frac{\delta_{lm} - 1_l p_m}{n^{2/3}} \right) \tag{D.11}$$

APPENDIX E: CHANGE OF VARIABLES: SCALAR GIBBS DERIVATIVES TO HELMHOLTZ DERIVATIVES

This appendix provides partial differential operators and partial derivatives required to calculate the second order partial differentials of the Helmholtz energy $\mathcal{F}$ under hydrostatic conditions. As done for the Helmholtz energy under non-hydrostatic conditions in Appendix C, we define a set of variables for the hydrostatic Helmholtz energy $(V', T', \boldsymbol{n}')$, and a modified set for the hydrostatic Gibbs energy $(P^{\mathcal{G}}, T^{\mathcal{G}}, \boldsymbol{n}^{\mathcal{G}})$. Any function can then be written:

$$\Phi(P^{\mathcal{G}}(V', T', \boldsymbol{n}'), T^{\mathcal{G}}(T'), \boldsymbol{n}^{\mathcal{G}}(\boldsymbol{n}')) \tag{E.1}$$

The partial differential operators for the Helmholtz variables are:

$$\frac{\partial}{\partial V'} = \frac{\partial P}{\partial V'} \frac{\partial}{\partial P^{\mathcal{G}}} \tag{E.2}$$

$$\frac{\partial}{\partial T'} = \frac{\partial T}{\partial T'} \frac{\partial}{\partial T^{\mathcal{G}}} + \frac{\partial P}{\partial T'} \frac{\partial}{\partial P^{\mathcal{G}}} \tag{E.3}$$

$$\frac{\partial}{\partial n_i'} = \frac{\partial}{\partial n_i^{\mathcal{G}}} + \frac{\partial P}{\partial n_i'} \frac{\partial}{\partial P^{\mathcal{G}}} \tag{E.4}$$

In order to express the second derivatives in their most compact form, we will use the following thermodynamic identities:

$$\frac{\partial P}{\partial V} = -\frac{K_T}{V} \tag{E.5}$$

$$\frac{\partial P}{\partial T} = \frac{\partial S}{\partial V} = \alpha_V K_T \tag{E.6}$$

A final relation is obtained by taking the total derivative of V and differentiating with respect to $\boldsymbol{n}'$:

$$dV = \frac{\partial V}{\partial P^{\mathcal{G}}} dP^{\mathcal{G}} + \frac{\partial V}{\partial T^{\mathcal{G}}} dT^{\mathcal{G}} + \frac{\partial V}{\partial n_i^{\mathcal{G}}} dn_i^{\mathcal{G}} \tag{E.7}$$

$$\frac{\partial V}{\partial n'_j} = \frac{\partial V}{\partial P^{\mathcal{G}}} \frac{\partial P}{\partial n'_j} + \frac{\partial V}{\partial T^{\mathcal{G}}} \frac{\partial T}{\partial n'_j} + \frac{\partial V}{\partial n_i^{\mathcal{G}}} \frac{\partial n_i}{\partial n'_j} \tag{E.8}$$

$$0 = \frac{\partial V}{\partial P^{\mathcal{G}}} \frac{\partial P}{\partial n'_j} + \frac{\partial V}{\partial n_j^{\mathcal{G}}} \tag{E.9}$$

$$\frac{\partial P}{\partial n'_j} = -\frac{\partial P}{\partial V} \frac{\partial V}{\partial n_j^{\mathcal{G}}} \tag{E.10}$$

Finally, the required second derivatives can be derived:

$$\frac{\partial P}{\partial n'_i} = \frac{K_T}{V} \frac{\partial V}{\partial n_i^{\mathcal{G}}} \tag{E.11}$$

$$\frac{\partial S}{\partial n'_i} = \frac{\partial S}{\partial n_i^{\mathcal{G}}} + \frac{\partial P}{\partial n'_i} \frac{\partial S}{\partial P^{\mathcal{G}}} \tag{E.12}$$

$$= \frac{\partial S}{\partial n_i^{\mathcal{G}}} + \left(-\frac{\partial P}{\partial V} \frac{\partial V}{\partial n_i^{\mathcal{G}}} \right) \frac{\partial S}{\partial P^{\mathcal{G}}} \tag{E.13}$$

$$= \frac{\partial S}{\partial n_i^{\mathcal{G}}} - \alpha_V K_T \frac{\partial V}{\partial n_i^{\mathcal{G}}} \tag{E.14}$$

$$\frac{\partial^2 \mathcal{F}}{\partial n'_i \partial n'_j} = \frac{\partial^2 \mathcal{G}}{\partial n'_i \partial n'_j} - V \frac{\partial^2 P}{\partial n'_i \partial n'_j} \tag{E.15}$$

$$= \frac{\partial^2 \mathcal{G}}{\partial n_i^{\mathcal{G}} \partial n_j^{\mathcal{G}}} + \frac{\partial P}{\partial n'_i} \frac{\partial^2 \mathcal{G}}{\partial P^{\mathcal{G}} \partial n_j^{\mathcal{G}}} + \frac{\partial P}{\partial n'_j} \frac{\partial^2 \mathcal{G}}{\partial P^{\mathcal{G}} \partial n_i^{\mathcal{G}}} + \frac{\partial P}{\partial n'_i} \frac{\partial P}{\partial n_j} \frac{\partial^2 \mathcal{G}}{\partial P^{\mathcal{G}} \partial P^{\mathcal{G}}} \tag{E.16}$$

$$= \frac{\partial^2 \mathcal{G}}{\partial n_i^{\mathcal{G}} \partial n_j^{\mathcal{G}}} + \frac{\partial V}{\partial n_i^{\mathcal{G}}} \left(\frac{K_T}{V} \right) \frac{\partial V}{\partial n_j^{\mathcal{G}}} + \frac{\partial V}{\partial n_j^{\mathcal{G}}} \left(\frac{K_T}{V} \right) \frac{\partial V}{\partial n_i^{\mathcal{G}}} - \frac{\partial V}{\partial n_i^{\mathcal{G}}} \left(\frac{K_T}{V} \right) \frac{\partial V}{\partial n_j^{\mathcal{G}}} \tag{E.17}$$

$$= \frac{\partial^2 \mathcal{G}}{\partial n_i^{\mathcal{G}} \partial n_j^{\mathcal{G}}} + \frac{\partial V}{\partial n_i^{\mathcal{G}}} \left(\frac{K_T}{V} \right) \frac{\partial V}{\partial n_j^{\mathcal{G}}} \tag{E.18}$$

APPENDIX F: CHANGE OF VARIABLES: ANISOTROPIC HELMHOLTZ DERIVATIVES TO INTERNAL ENERGY DERIVATIVES

This appendix provides partial differential operators and partial derivatives required to calculate the second order partial differentials of the internal energy $\mathcal{E}$ as functions of partial derivatives of the Helmholtz energy $\mathcal{F}$. We define a "natural" set of variables for the Helmholtz energy in the small strain case $(\boldsymbol{\varepsilon}, T, \boldsymbol{n})$, and a modified set for the internal energy $(\boldsymbol{\varepsilon}^{\mathcal{E}}, S^{\mathcal{E}}, \boldsymbol{n}^{\mathcal{E}})$. Any function can be written

$$\Phi(\boldsymbol{\varepsilon}(\boldsymbol{\varepsilon}^{\mathcal{E}}), T(\boldsymbol{\varepsilon}^{\mathcal{E}}, S^{\mathcal{E}}, \boldsymbol{n}^{\mathcal{E}}), \boldsymbol{n}(\boldsymbol{n}^{\mathcal{E}})) \tag{F.1}$$

The partial differential operators for the modified set of variables are:

$$\frac{\partial}{\partial \varepsilon_{ij}^{\mathcal{E}}} = \delta_{ik}\delta_{jl}\frac{\partial}{\partial \varepsilon_{kl}} + \frac{\partial T}{\partial \varepsilon_{ij}^{\mathcal{E}}}\frac{\partial}{\partial T} \tag{F.2}$$

$$\frac{\partial}{\partial S^{\mathcal{E}}} = \frac{\partial T}{\partial S^{\mathcal{E}}}\frac{\partial}{\partial T} \tag{F.3}$$

$$\frac{\partial}{\partial n_i^{\mathcal{E}}} = \delta_{ij}\frac{\partial}{\partial n_j} + \frac{\partial T}{\partial n_i^{\mathcal{E}}}\frac{\partial}{\partial T} \tag{F.4}$$

In order to express the second derivatives in their most compact form, we will use the following thermodynamic identity:

$$\frac{\partial T}{\partial S} = \frac{C_\varepsilon}{T} \tag{F.5}$$

Further relations are obtained by differentiating S with respect to the $\boldsymbol{\varepsilon}^{\mathcal{E}}$, $S^{\mathcal{E}}$ and $\boldsymbol{x}^{\mathcal{E}}$:

$$dS = \frac{\partial S}{\partial \varepsilon_{ij}}d\varepsilon_{ij} + \frac{\partial S}{\partial T}dT + \frac{\partial S}{\partial n_i}dn_i \tag{F.6}$$

$$\frac{\partial T}{\partial \varepsilon_{ij}^{\mathcal{E}}} = -\frac{T}{C_\varepsilon}\frac{\partial S}{\partial \varepsilon_{ij}} \tag{F.7}$$

$$\frac{\partial T}{\partial S^{\mathcal{E}}} = \frac{C_\varepsilon}{T} \tag{F.8}$$

$$\frac{\partial T}{\partial n_i^{\mathcal{E}}} = -\frac{T}{C_\varepsilon}\frac{\partial S}{\partial n_i} \tag{F.9}$$

Finally, the required second derivatives can be derived:

$$\frac{\partial^2 \mathcal{E}}{\partial n_i^{\mathcal{E}}\partial S^{\mathcal{E}}} = \frac{\partial T}{\partial n_i^{\mathcal{E}}} = -\frac{T}{C_\varepsilon}\frac{\partial S}{\partial n_i} = \frac{T}{C_\varepsilon}\frac{\partial^2 \mathcal{F}}{\partial n_i \partial T} \tag{F.10}$$

$$\frac{\partial^2 \mathcal{E}}{\partial n_i^{\mathcal{E}}\partial \varepsilon_{jk}^{\mathcal{E}}} = \frac{\partial \sigma_{jk}}{\partial n_i^{\mathcal{E}}} = \frac{\partial^2 \mathcal{F}}{\partial n_i \partial \varepsilon_{jk}} - \frac{T}{C_\varepsilon}\frac{\partial S}{\partial n_i}\frac{\partial^2 \mathcal{F}}{\partial T \partial \varepsilon_{jk}} = \frac{\partial^2 \mathcal{F}}{\partial n_i \partial \varepsilon_{jk}} + \frac{VT\pi_{jk}}{C_\varepsilon}\frac{\partial^2 \mathcal{F}}{\partial n_i \partial T} \tag{F.11}$$

$$\frac{\partial^2 \mathcal{E}}{\partial n_i^{\mathcal{E}}\partial n_j^{\mathcal{E}}} = \frac{\partial^2 \mathcal{F}}{\partial n_i^{\mathcal{E}}\partial n_j^{\mathcal{E}}} + S\frac{\partial^2 T}{\partial n_i^{\mathcal{E}}\partial n_j^{\mathcal{E}}} \tag{F.12}$$

$$= \frac{\partial^2 \mathcal{F}}{\partial n_i \partial n_j} + \frac{\partial T}{\partial n_i^{\mathcal{E}}}\frac{\partial^2 \mathcal{F}}{\partial n_j \partial T} + \frac{\partial T}{\partial n_j^{\mathcal{E}}}\frac{\partial^2 \mathcal{F}}{\partial n_i \partial T} + \frac{\partial T}{\partial n_i^{\mathcal{E}}}\frac{\partial^2 \mathcal{F}}{\partial T \partial T}\frac{\partial T}{\partial n_j^{\mathcal{E}}} \tag{F.13}$$

$$= \frac{\partial^2 \mathcal{F}}{\partial n_i \partial n_j} + \frac{\partial T}{\partial n_i^{\mathcal{E}}}\frac{\partial^2 \mathcal{F}}{\partial n_j \partial T} + \frac{\partial T}{\partial n_j^{\mathcal{E}}}\frac{\partial^2 \mathcal{F}}{\partial n_i \partial T} - \frac{\partial T}{\partial n_i^{\mathcal{E}}}\frac{\partial S}{\partial T}\frac{\partial T}{\partial n_j^{\mathcal{E}}} \tag{F.14}$$

$$= \frac{\partial^2 \mathcal{F}}{\partial n_i \partial n_j} + \frac{T}{C_\varepsilon}\frac{\partial S}{\partial n_i}\frac{\partial S}{\partial n_j} + \frac{T}{C_\varepsilon}\frac{\partial S}{\partial n_j}\frac{\partial S}{\partial n_i} - \frac{T}{C_\varepsilon}\frac{\partial S}{\partial n_j}\frac{\partial S}{\partial n_i} \tag{F.15}$$

$$= \frac{\partial^2 \mathcal{F}}{\partial n_i \partial n_j} + \frac{\partial S}{\partial n_i}\frac{T}{C_\varepsilon}\frac{\partial S}{\partial n_j} \tag{F.16}$$

$$= \frac{\partial^2 \mathcal{F}}{\partial n_i \partial n_j} + \frac{\partial^2 \mathcal{F}}{\partial n_i \partial T}\frac{T}{C_\varepsilon}\frac{\partial^2 \mathcal{F}}{\partial n_j \partial T} \tag{F.17}$$

This paper has been produced using the Blackwell Scientific Publications GJI LaTeX2e class file.